Helsinki University of Technology Publications in Engineering Physics
Teknillisen korkeakoulun teknillisen fysiikan julkaisuja
Espoo 2000 TKK-F-A804

ANALYSIS AND MODELING OF SURFACE-ACOUSTIC WAVE RESONATORS

Julius Koskela

Dissertation for the degree of Doctor of Science in Technology to be presented with due permission of the Department of Engineering Physics and Mathematics for public examination and debate in Auditorium F1 at Helsinki University of Technology (Espoo, Finland) on the 12th of January, 2001, at 12 o´clock noon.

Helsinki University of Technology
Department of Engineering Physics and Mathematics
Materials Physics Laboratory

Teknillinen korkeakoulu
Teknillisen fysiikan ja matematiikan osasto
Materiaalifysiikan laboratorio

Distribution:
Helsinki University of Technology
Materials Physics Laboratory
P.O. Box 2200
FIN-02015 HUT
Tel. +358-9-451 3150
Fax. +358-9-451 3164
E-mail: julius@focus.hut.fi

ISBN 951-22-5276-7
ISSN 1456-3320

Otamedia Oy
Espoo 2000

Preface

This work was carried out in the Materials Physics Laboratory at Helsinki University of Technology in collaboration with Micronas Semiconductor SA and with Thomson Microsonics, Neuchâtel, Switzerland and Sophia-Antipolis, France.

This work summarizes a working period of four years, during which I have received support and encouragement from many persons. Discussions with Ari Alastalo, Tero Heikkilä, Teemu Pohjola, Dr. Sergei Popov, Simo Sääskilahti, Professor Jan Westerholm, and Dr. Pekka Äyräs have been most enjoyable and they are warmly recognized. I wish to thank the personnel at the Materials Physics Laboratory for a pleasant working environment.

The technical discussions with Dr. Juha Fagerholm, Dr. Sergei Kondratyev, Dr. David Morgan, Janne Salo, Dr. Marc Solal, and Dr. Thor Thorvaldsson have been most beneficial. It is my pleasure and honour to thank Clinton Hartmann, Professor Ken-ya Hashimoto, Katri Honkanen, Jouni Knuuttila, Saku Lehtonen, Tapani Makkonen, and Pasi Tikka for fruitful collaboration and coauthoring.

I am deeply grateful, as a person and as a scientist, to my instructor Professor Victor Plessky, for sharing his insight on the discipline of surface acoustic, and for his belief and devotion on our research. It is a priviledge to have worked with him all this time.

I am deeply indebted to my supervisor Professor Martti Salomaa, for the opportunity to work in the field and for the excellent working conditions. Without his determination the research group would not exist. His worthful trust and patience on me are highly appreciated.

Scholarships and financial support from Helsinki University of Technology, Micronas Semiconductor SA, TEKES, and NOKIA Foundation are gratefully acknowledged. Especially, I thank the Academy of Finland for a fellowship within the graduate school in Technical Physics.

Finally, I would like to thank my family, my friends—including those already mentioned—and Anne for their presence in my life.

List of Publications

This dissertation is a review of the author's work in the field of surface-acoustic wave technology. It consists of an overview and the following selection of publications in this field:

I J. Koskela, V. P. Plessky, and M. M. Salomaa, "Suppression of the leaky SAW attenuation with heavy mechanical loading", *IEEE Transactions on Ultrasonics, Ferroelectrics, and Frequency Control* **45**, 439-449 (1998).

II J. Koskela, S. Lehtonen, V. P. Plessky, and M. M. Salomaa, "Surface tranverse waves on langasite", *Applied Physics Letters* **72**, 2665-2667 (1998).

III J. Koskela, V. P. Plessky, and M. M. Salomaa, "SAW/LSAW COM parameter extraction from computer experiments with harmonic admittance of a periodic array of electrodes", *IEEE Transactions on Ultrasonics, Ferroelectrics, and Frequency Control* **46**, 806-816 (1999).

IV J. Koskela, V. P. Plessky, and M. M. Salomaa, "Theory for shear horizontal surface acoustic waves in finite synchronous resonators", *IEEE Transactions on Ultrasonics, Ferroelectrics, and Frequency Control* **47**, 1550-1560 (2000).

V J. Koskela, J. V. Knuuttila, P. T. Tikka, C. S. Hartmann, V. P. Plessky, and M. M. Salomaa, "Mechanism for acoustic leakage in surface-acoustic wave resonators on rotated Y-cut lithium tantalate substrate", *Applied Physics Letters* **75**, 2683-2685 (1999).

VI J. Koskela, J. V. Knuuttila, T. Makkonen, V. P. Plessky, and M. M. Salomaa, "Acoustic loss mechanisms in leaky SAW resonators on lithium tantalate", *Report TKK-F-A801*, ISBN 951-22-5142-6, submitted to *IEEE Transactions on Ultrasonics, Ferroelectrics, and Frequency Control* (2000).

Throughout the overview, these publications are referred to by their Roman numerals.

Author's Contribution

The studies in this dissertion are the result of work carried in the Materials Physics Laboratory at Helsinki University of Technology (HUT) during the years 1996-2000. Papers I-III were conducted in collaboration with Micronas Semiconductor SA, Bevaix, Switzerland, while papers IV-VI involve cooperation with Thomson Microsonics, SAW Design Bureau, Neuchâtel, Switzerland. Paper V results from discussions with Clinton S. Hartmann, RF SAW Components, Dallas, Texas, USA.

The author has substantially contributed to the research in Papers I-VI. He has developed and formulated a significant part of the theoretical methods in Papers III, IV, and VI. All theoretical calculations, programming, and numerical computations in Papers I-VI were carried out by him. The author actively participated in the writing of Paper II; Papers I, III-VI were written mainly by him. Considerable part of the results covered in Papers I-VI has been presented in international conferences, the results in Papers III and IV by the author and those in Papers V and VI by the author and collaborators.

Contents

1 Introduction

The last two decades have witnessed a furious growth of the telecommunication industry. Among the technical prerequisites for modern cellular and cordless systems are radio-frequency (RF) filters with very small size and minimal losses. To meet this demand, a novel class of components based on the surface-acoustic wave (SAW) technology has emerged. A work of art in miniaturization, the SAW technology combines sophisticated engineering with the inherent materials physical properties of the covalent crystals known as piezoelectrics.

Surface-acoustic waves are acoustic waves propagating in an elastic substrate medium. In constrast to plane-wave like bulk-acoustic waves (BAWs), SAWs are localized to the surface of the substrate with most of their energy confined to within a few wavelengths from the surface. Since their discovery in 1885 by Lord Rayleigh [1], the surface-acoustic waves have been of interest to physics, seismology, and component technology within military and civil applications.

Due to their localization to the surface, the surface-acoustic waves are sensitive to—and, therefore: easily generated and manipulated by—structures on the surface of the substrate. Within this work, piezoelectric crystal substrates are considered; in piezoelectric materials, the electrical and mechanical fields are mutually coupled [2]. A typical SAW device consists of a pattern of electrodes fabricated atop a piezoelectric crystal wafer using lithographic processes similar to those used in the semiconductor industry. The basic element of a SAW device is an interdigital transducer (IDT) [3], illustrated in Fig. 1.1. The operation of the IDT is based on the piezoelectric effect: as a voltage is applied between the busbars of the IDT, the electric field between the electrodes penetrates into the substrate and, due to the piezoelectric coupling, acoustic waves are excited. Reciprocally, the acoustic waves accumulate electric charge on

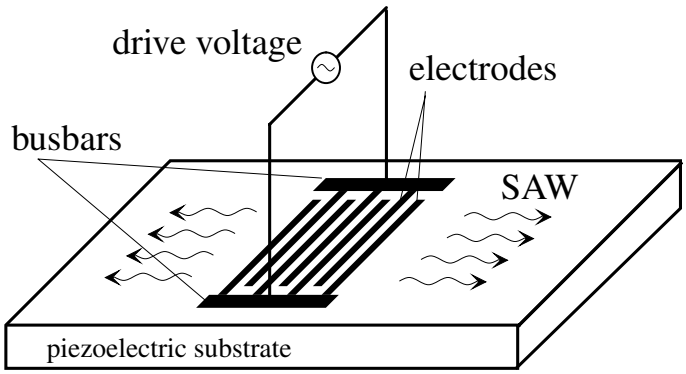

Figure 1.1: Interdigital transducer (IDT) serves as an antenna for launching and receiving surface-acoustic waves. The device is bidirectional: waves are launched both to the left and to the right from the IDT.

the electrodes, *i.e.* they generate currents. The accumulated charges lead to a secondary excitation of acoustic waves. Hence, the IDT may simultaneously operate as a transmitter, a receiver and a reflector of acoustic waves.

Traditionally, surface-acoustic wave devices have been used, for example, in high-performance delay lines and transversal filters [4], resonators [5–10], acoustic convolvers [11, 12], and reflective array compressors [4]. The conventional SAW filter concept is based on the frequency-dependent conversion of the electric signal into an acoustic wave with an IDT, followed by a reconversion into an electric signal with another IDT. Due to the bidirectionality of the IDT, the conventional SAW filters have a minimum insertion loss of 6 dB. Additional losses occur due to designing for optimal frequency characteristics, resulting in a typical loss level of 15-25 dB. Losses, the poor power tolerance, and the rather extended device length render transversal filters totally unfit for applications within mobile systems.

New emerging applications of the SAW technology include SAW sensors [13] and tags [14] but, indeed, recent advantages in SAW technology have been driven by the vast expansion of the cellular phone markets. To meet the stringent requirements set by the industry, a new generation of SAW filters has emerged. Modern RF SAW filters typically feature minuscule size, an insertion loss within few dB, and an operating frequency up to 2 GHz and above. There are various design approaches for low-loss devices, but some main approaches may be classified: impedance element filters [15–19] (IEFs), coupled resonator filters [20–22], transversally coupled resonator filters [23–25], and interdigitated IDT structures [26, 27].

The working principles of these modern RF SAW devices differ essentially from those of the conventional transversal filters. Due to the high operating frequencies, the electrode thickness is not negligible in comparison to the acoustic wavelength. Consequently, the mass loading by the electrodes is significant, resulting in slowing of the wave and, most importantly, in reflections. When the wavelength of an acoustic wave is close to a multiple of the grating periodicity, a strong interaction between the counterpropagating waves takes place and the acoustic field is governed by the arising Bragg reflections. These serve to trap the acoustic energy inside the device. For this reason–in contrast to the transversal filters–the finite reflectivity of the electrodes is fundamental to the device operation.

The design of high-performance SAW devices requires precise simulation models. This work is concerned about the simulation of the excitation and propagation of surface-acoustic waves in periodic electrode structures. Of special interest is the synchronous uniform one-port SAW resonator illustrated in Fig. 1.2(a). It consists of a (typically long) IDT and two electrically shorted gratings, which serve as additional reflectors. The main electrical characteristic of the device is a strong resonance-antiresonance pattern in the frequency response, see Fig. 1.2(b). Due to the large impedance difference between the resonance and the antiresonance, the structure works as a frequency-controlled switch—an impedance element (IE). Using such IEs as building blocks in electrical networks, various impedance element filters (IEFs) may be constructed [28], as shown in Fig. 1.3.

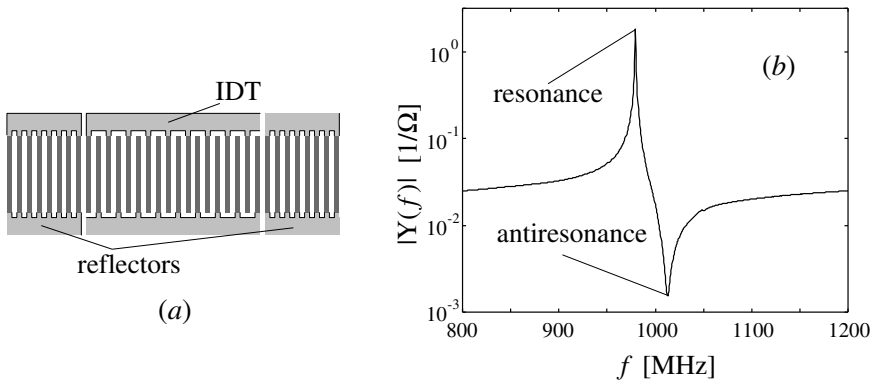

Figure 1.2: (a) Schematical synchronous uniform SAW resonator and (b) a measured frequency response, featuring a resonance at 980 MHz, an antiresonance at 1013 MHz, and, between these, an impedance level difference of about three magnitudes.

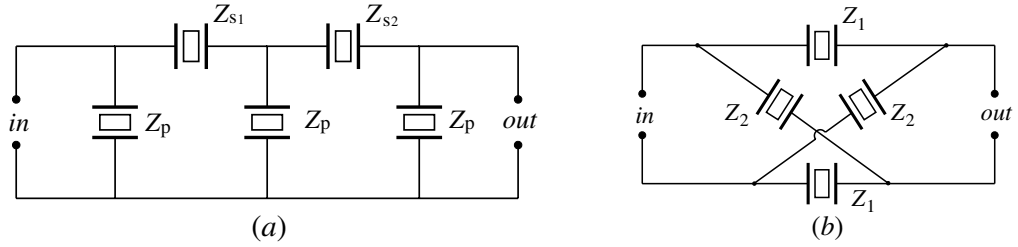

Figure 1.3: Schematic impedance element filters: (a) ladder filter and (b) balanced-bridge filter. Each component shown in the network is an impedance element: a synchronous one-port SAW resonator with frequency-dependent impedance $Z(f)$.

Interest in rigorous CAD tools for device design is increasing but, at the moment, such methods are too slow to be used as the primary means of design. However, infinite periodic electrode arrays may be simulated rather effortlessly. In Papers I-III of this work we have implemented such a simulator and applied it to study leaky surface-acoustic wave resonators on lithium niobate and lithium tantalate substrates and surface transverse wave resonators on langasite substrate. The computer simulations provide an inexpensive and reliable method for the characterization and optimization of the substrate-electrode combinations. The analyses are based on the concept of harmonic admittance, developed by Bløtekjær *et al.* [29,30] and reformulated by Zhang *et al.* [31]. Their theory is reviewed in Chapter 2, while Chapter 3 concentrates on the Papers I-III.

Since rigorous simulations cannot be used as the main tool in device design, phenomenological models such as the coupling-of-modes (COM) model [32], the P-matrix formalism [33], and equivalent circuit models, are commonly resorted to. These are less accurate than rigorous models but considerable faster and, hence, they may be used with optimization algorithms. The comparison of these phenomenological models [34] reveals that, under the same conditions, almost identical results are obtained–

and the same difficulties are encountered–with all of them. Within this work, only the COM formalism is explicitly referred to.

The coupling-of-modes formalism has been extensively used since 1950's in various problems related to optics and electromagnetism [35,36]. It proved appropriate for the analysis of SAW gratings [37, 38], uniform transducers [39–42], and spatially varying structures [32]. The accuracy of the COM theory (and other phenomenological models) depends crucially on explicit model parameters, which describe properties such as wave velocity, reflectivity from the electrodes, the strength of the electromechanical coupling, and the capacitance of the structure. For successful device design these parameters must be known to high accuracy.

The parameters may be achieved in various ways. The electrical measurements from special test structures [43, 44] seem to be the most reliable method. Unfortunately, since the parameters have to be individually determined for each substrate with every material, size, shape, and structure of the electrodes, the experimental approach is both expensive and time-consuming. Moreover, uncertainties in the properties and the geometry of the electrodes due to the manufacturing technology limit the accuracy of the results obtained. For this reason, numerical techniques for parameter extraction have recently been developed. In Paper III of this work we propose an algorithm for efficient COM parameter extraction from the harmonic admittance of an infinite electrode array. The method is also discussed in Chapter 3.

Despite their intrinsic simplicity, with accurately measured parameters the COM theory and the analogous models can be astonishingly precise for narrow-band devices employing classical SAWs on, for example, ST-cut quartz. However, the model is considerably less accurate for shear-horizontally polarized surface-acoustic waves (SH-SAWs), such as surface transverse waves (STWs), and the leaky surface-acoustic waves (LSAWs) on rotated $LiNbO_3$ and $LiTaO_3$ substrates. The latter are employed extensively in modern RF SAW filters. In Paper IV we construct a phenomenological theory for the simulation of synchronous uniform SH-SAW resonators. This model is reviewed in Chapter 4.

Further discrepancies between simulations and experiments arise due to numerous acoustic phenomena such as dispersion, scattering into bulk-acoustic waves, and waveguiding effects, and due to parasitic effects such as resistive losses, stray capacitances, and the inductances of the bonding wires. In Papers V and VI we have analyzed acoustic loss mechanisms in synchronous LSAW resonators in rotated Y-cut $LiTaO_3$ substrates. The results are reviewed in Chapter 5.

Discussion and the conclusions are provided in Chapter 6.

2 Periodic Electrode Array

The periodic array of electrodes illustrated in Fig. 2.1 constitutes an archetypal periodic structure. The electrical connections may be arbitrary: the excitation and propagation of acoustic waves in the array and the electric response of the structure subject to various electric configurations are of fundamental interest in theoretical SAW analysis. Zhang *et al.* [31] were able to show that the complete description of the electric response is contained in a single function, the harmonic admittance of the electrode array. The concept was originally introduced as "strip admittance" by Bløtekjær *et al.* [29,30]. Zhang *et al.* elegantly reformulated the theory and relabeled the function "harmonic admittance".

The harmonic admittance is employed extensively in this work. This Chapter serves as an introduction to the concept, first reviewing the theory of Zhang and coworkers and then outlining how the function may be applied in the analysis and simulation of SAW devices.

2.1 Harmonic and Mutual Admittances

Following Ref. [31], let V_n denote the electric potential on electrode n, defined with respect to some reference level, and let I_m denote the resulting current on electrode m. Throughout this work, harmonic time dependence at the angular frequency $\omega=2\pi f$ is assumed, with the factor $e^{i\omega t}$ being subsumed.

The currents are linearly related to the electrode potentials. The proportionality coefficients

$$y_{mn}(f) = \frac{\partial I_n}{\partial V_m} \tag{2.1}$$

are called mutual admittances. Due to the translational invariance of the array the mutual admittances cannot depend on the absolute electrode locations m and n: they must be functions of the difference $m-n$. Denote y_{mn} by y_{m-n}. Owing to reciprocity $y_m=y_{-m}$ [31].

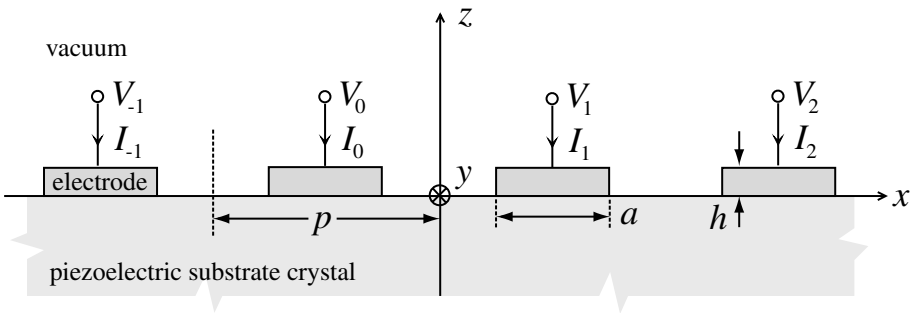

Figure 2.1: Periodic array of electrodes on a piezoelectric substrate crystal.

Since the array must remain charge neutral under arbitrary excitation, the mutual admittances satisfy

$$\sum_{m=-\infty}^{+\infty} y_m = 0. \tag{2.2}$$

Consequently, the reference level for electrode potentials may be chosen arbitrarily. The currents resulting from an arbitrary voltage configuration are obtained using linear superposition:

$$I_n = \sum_{m=-\infty}^{+\infty} y_{m-n}(f) V_m. \tag{2.3}$$

Hence, the mutual admittances y_m fully characterize the electric response of the structure. In principle, the mutual admittances could be determined from the electrode currents under a unitary excitation of the array, see Fig. 2.2(a). However, the unitary excitation breaks the translational symmetry of the infinite electrode array, which would be beneficial for efficient numerical computations. Zhang *et al.* discovered that the same information can be deduced from the response of the array to the harmonic excitation, see Fig. 2.2(b).

Under γ-harmonic excitation, the electrode potentials assume the form

$$V_n = V_0\, e^{-i2\pi\gamma n}. \tag{2.4}$$

Substituting the voltages from Eq. (2.4) into Eq. (2.3), it is found that the currents also have γ-harmonic form. The ratio

$$\tilde{Y}(\gamma, f) = \frac{I_n}{V_n} = \frac{I_0}{V_0} = \sum_{m=-\infty}^{+\infty} y_m(f)\, e^{-i2\pi\gamma m} \tag{2.5}$$

is called the harmonic admittance. Evidently, it is a periodic function of γ with the periodicity $\tilde{Y}(\gamma+1, f) = \tilde{Y}(\gamma, f)$. Since a constant voltage does not excite waves, the function vanishes for integer values of γ. Furthermore, owing to the reciprocity of the mutual admittances, the harmonic admittance is symmetric about γ=0.5.

Based on Eq. (2.5), the harmonic admittance may be interpreted as a discrete Fourier transform of the mutual admittances. Reciprocally, the mutual admittances

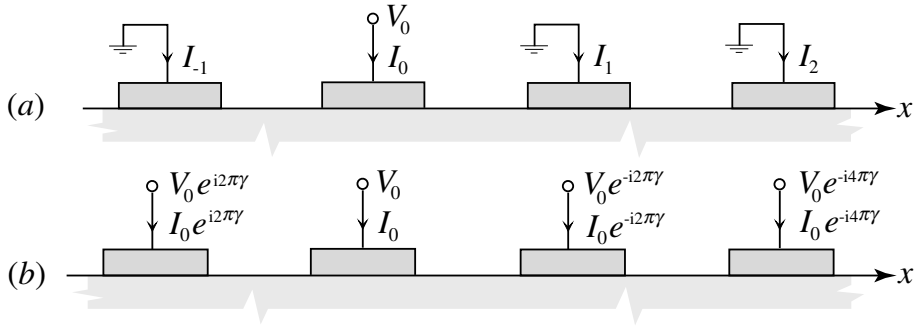

Figure 2.2: (a) Unitary and (b) harmonic excitation of the periodic electrode array.

may be computed from the harmonic admittance as

$$y_m(f) = \int_0^1 \tilde{Y}(\gamma, f)\, e^{i2\pi\gamma m} d\gamma. \tag{2.6}$$

In contrast to unitary excitation, harmonic excitation is most suitable for numerical computations. The treatment is applicable for arbitrary apertures and it may be generalized for more complicated periods [45].

2.2 Applications of Harmonic Admittance

Conceptually, methods for the analysis of periodic electrode structures may be classified into two principal categories: the analyses of the eigenmode problems and those of the generation problems. In the eigenmode problems, waves propagating under the boundary conditions of electrically open or shorted electrodes are sought. The phase shift, *i.e.*, wavenumber, in the elastic and electric fields between the successive periods is to be found as a function of frequency; as a result, the dispersion curves are obtained. A limitation of this method is that the coupling to an applied voltage can be analyzed only indirectly [42]. Moreover, complex-valued wavenumbers have to be considered, which requires a somewhat complicated complex-analytic treatment [46].

An alternative to the eigenmode analysis is the generation analysis. The generation approach may be understood as a simulated experiment: the system modeled is driven by a voltage source, and the interest lies in the currents on the electrodes. Since the generation formulation closely resembles experiments, the results obtained are easier to interpret than those of the eigenmode scheme.

For example, the admittance of a long synchronous one-port resonator may be simulated as an infinite electrode array under finite electric excitation [47, 48], see Fig. 2.3. Close to the stopband frequencies the acoustic field in the resonator is localized to the IDT area and the reflectors are well approximated by infinite gratings. The admittance of the constructed infinite resonator may be obtained from Eq. (2.3) by summing the currents in the electrodes on one of the two busbars. For numerical simulations, it is convenient to utilize Eq. (2.6) and to express the admittance as a weighted integral over the harmonic admittance. For the example in Fig. 2.3, one finds

$$Y_{N_\mathrm{p}}(f) = \sum_{n=1}^{N_\mathrm{p}} \sum_{m=1}^{N_\mathrm{p}} y_{2m-2n} = \int_0^1 \tilde{Y}(\gamma, f) \frac{\sin^2(2\pi\gamma N_\mathrm{p})}{\sin^2(2\pi\gamma)} d\gamma. \tag{2.7}$$

The simpliest and perhaps the most important generation problem is that of harmonic excitation with γ=1/2. The potentials in the consequtive electrodes are of the form $V_n = (-1)^n$. Hence, the structure may be interpreted as an infinite resonator at the limit of an infinite single-electrode transducer:

$$\tilde{Y}\left(\tfrac{1}{2}, f\right) = \lim_{N_\mathrm{p}\to\infty} 2Y_{N_\mathrm{p}}(f)/N_\mathrm{p}. \tag{2.8}$$

Since electrically active eigenmodes contribute to the response of the array to an electric excitation, the eigenmode and generation approaches are not independent. In

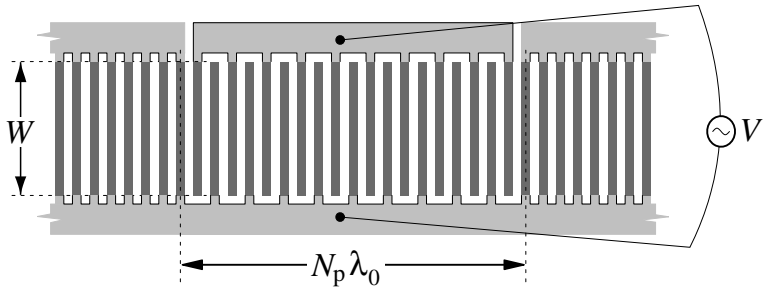

Figure 2.3: An infinite one-port resonator: an IDT with N_p electrode pairs and two infinite reflectors, formed from a periodic electrode array by finite electric excitation. In this example, the reflectors are connected to the lower busbar which may be considered grounded.

particular, the eigenmodes of the electrically short-circuited (sc) and open-circuited (oc) arrays manifest themselves as the poles and zeros of the harmonic admittance, respectively. Consequently, the harmonic admittance may be interpreted as the ratio of the dispersion relation for open and shorted gratings:

$$Y(\gamma, f) = \frac{D_\mathrm{oc}(\gamma, f)}{D_\mathrm{sc}(\gamma, f)}. \tag{2.9}$$

The conditions D_oc=0 and $D_\mathrm{sc} = 0$ respectively define the dispersion relations for the open-circuited and short-circuited structures. A rigorous mathematical proof of this theorem was recently found by Biryukov [49]. The functions $D_\mathrm{oc}(\gamma, f)$ and $D_\mathrm{sc}(\gamma, f)$ may be obtained as the determinants of appropriately defined systems of equations obtained, *e.g.*, from numerical computations with the boundary-element method. The branch points of the harmonic admittance may be identified with bulk-acoustic waves with their energy propagating along the surface.

2.3 Harmonic Admittance in the Present Work

The concepts of periodic electrode array and harmonic admittance are applied extensively in this work. We have formulated a rigorous simulator for arrays with an infinite aperture (Papers I and III) and applied it to characterize SAW excitation in various substrates (Papers I and II). Procedure for extracting phenomenological parameters based on the rigorous simulations has been developed (Paper III). A phenomenological model for finite surface transverse wave (STW) resonators is formed by first constructing a formalism for STWs in a periodic electrode array and, subsequently, by taking into account the reflections from the edges of the reflectors (Paper IV). Extending the periodic STW model for finite apertures and employing Eq. (2.7) enables quantitative analyses of the loss mechanisms in infinite waveguide resonators (Paper VI).

3 Rigorous Simulation

The properties of surface-acoustic wave devices strongly depend on the selection of the substrate material, crystal cut, and the height, width, and shape of the electrodes, and also on temperature. Determination of the SAW characteristics from test-structure measurements [43, 44] is laborous, time-consuming and, if rare or entirely new substrates are involved, very expensive. For this reason, reducing the number of experiments via numerical simulations seems attractive. We have implemented a simulation tool for infinite periodic electrode arrays and employed it to study the SAW characteristics on various substrates. One particularly important form of structure characterization is the extraction of the parameters used in the phenomenological design models. We have developed an efficient method for the extraction of the COM parameters from the rigorously computed harmonic admittance.

3.1 Field-Theoretical Formulation

Physically, the structure in Fig. 2.1 may be taken to consist of the piezoelectric substrate crystal, the metal electrodes on the crystal surface, and the surrounding vacuum. As simplifying approximations, the substrate is assumed semi-infinite, to fulfill the lower halfspace $z \leq 0$, and the electrodes are assumed infinitely thin from the electric point of the view. The substrate and the electrodes may be treated using the theory of elasticity [50, 51], the thermodynamical theory of piezoelectricity [52], and Maxwell's equations, while only Maxwell's equations are required for the vacuum.

The theory of elasticity considers a homogeneous continuous medium. The field quantities of interest are the mechanical displacement field $\vec{u}$, the electric field $\vec{E}$ and the magnetic field $\vec{B}$. In linear, piezoelectric media, the stress tensor and the electric displacement field $\vec{D}$ are linearly coupled to the strain tensor and to the electric field $\vec{E}$. Due to the low velocity of the acoustic waves, in comparison to the speed of light, the magnetic field may in practice be neglected. Consequently, the electric field may be approximated as the gradient of an oscillating electric potential ϕ:

$$\vec{E} = -\nabla\phi. \tag{3.1}$$

This is known as the quasistatic approximation. Within the quasistatic approximation, the constitutive relations are [52]

$$\begin{cases} T_{ij} = \sum\limits_{k,l=1}^{3} c^{E}_{ijkl} \dfrac{\partial u_k}{\partial x_l} + \sum\limits_{k=1}^{3} e_{kij} \dfrac{\partial \phi}{\partial x_k}, \\ D_i = \sum\limits_{j,k=1}^{3} e_{ijk} \dfrac{\partial u_j}{\partial x_k} - \sum\limits_{j=1}^{3} \varepsilon^{S}_{ij} \dfrac{\partial \phi}{\partial x_j}. \end{cases} \tag{3.2}$$

Here, x_1,x_2,x_3 denote the Cartesian coordinates x, y, z, respectively, T_{ij} are the components of the second-rank stress tensor, c_{ijkl} are the components of the fourth-rank

stiffness tensor, e_{ijk} are the components of the third-rank piezoelectric tensor, and ε_{ij} are the components of the second-rank permittivity tensor. The superscripts E and S indicate that the components of the tensors are to be measured under constant electric field and under constant strain, respectively.

The governing equations in the substrate and in the electrodes are the equations of motion (Newton's law)

$$-\rho\omega^2 u_i = \sum_{j=1}^{3} \frac{\partial T_{ij}}{\partial x_j}, \tag{3.3}$$

and Maxwell's equation

$$\nabla \cdot \vec{D} = 0. \tag{3.4}$$

Here, ρ denotes the mass density, and harmonic time dependence at the angular frequency ω is assumed. In vacuum, the electric displacement field is given by $\vec{D}{=}\varepsilon_0\vec{E}$, where ε_0 is the permittivity of vacuum, and the Maxwell equation reduces to

$$\nabla^2\phi = 0. \tag{3.5}$$

The mechanical boundary conditions are that: (1) the mechanical displacement field is continuous across the electrode-substrate interfaces; (2) the normal component of the stress tensor is continuous across the electrode-substrate interfaces; and (3) the normal component of the stress tensor vanishes on free surfaces, *i.e.*, on surfaces surrounded by vacuum.

The discontinuity of the normal component of the electric displacement across the electrode-substrate interface yields the surface charge density σ:

$$\sigma(x) = D_z^{\text{vacuum}}(x,0) - D_z^{\text{substrate}}(x,0). \tag{3.6}$$

The electrical boundary conditions are that: (4) the electric potential is continuous everywhere; (5) the electric potential is constant on the electrodes

$$\phi(x,0) = \phi_n, \qquad x \in [\, np{-}a/2, np{+}a/2\,], \tag{3.7}$$

and the potential difference between any two electrodes n and m must agree with the corresponding voltage difference defined by the electric excitation of the array,

$$\phi_n - \phi_m = V_n - V_m, \tag{3.8}$$

(6) the surface charge density must vanish at substrate-vacuum interfaces; and (7) the system remains charge neutral.

The radiation condition states that: (8) all energy originates from the crystal surface and the electrodes: the fields cannot grow towards $z \to \pm\infty$ and energy cannot be radiated from the infinities to the surface.

Once the geometry of the electrodes, the voltage differences, and the materials parameters (the mass density and the components of the stiffness tensor, piezoelectric tensor and permittivity tensor) are specified, the definition of the problem is complete. In principle, it only remains to solve the fields under the γ-harmonic excitation and to integrate the surface charge density over the electrode-substrate interface to obtain the oscillating net charge and, subsequently, the harmonic admittance.

3.2 Numerical Solution of the Field Equations

Due to the mechanical periodicity of the array and the properties of harmonic excitation, the computations may be reduced to only one reference period. In addition, the structure and the fields are virtually always assumed invariant along y, such that the problem reduces into a two-dimensional one. Nevertheless, solving for the mechanical and electrical fields requires sophisticated numerical techniques.

There exists an immense amount of literature on the numerical approaches. However, within the most prevalent methods currently in use, the fields in the substrate are modeled with the finite-element (FEM) method [53, 54], space harmonics expansion [55], Green's function techniques [56, 57] using the boundary-element method (BEM) [58,59,47,60–65], or both FEM and the space harmonics expansion [66]. Generalization of the Green's function methods for substrates covered by thin films is straightforward [67]. Due to the large relative electrode thicknesses used in modern RF SAW filters, the stresses in the electrode-substrate interface must be also computed rather precisely. The most popular approach is probably the versatile FEM [53, 54, 59, 47, 60–63, 66] although both the space harmonic expansion [55] and the normal mode expansion [64] have also been reported. A FEM/BEM-based simulator capable of treating multi-electrode unit periods has been developed and generously made available to SAW researchers by K. Hashimoto [45].

We have formulated and implemented a FEM/BEM-based method for computing the harmonic admittance (Papers I and III) for an arbitrary substrate crystal, crystal cut, and the width, thickness, and material of the trapezoidal electrodes, see Fig. 3.1. This code forms the backbone of the analyses and applications in Papers I-III.

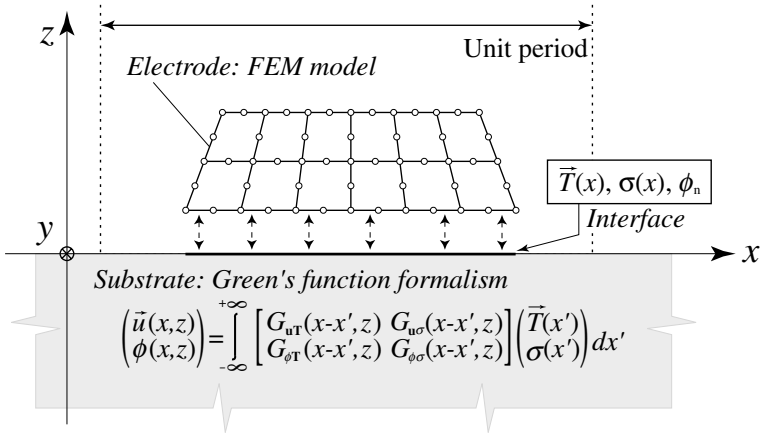

Figure 3.1: In FEM/BEM models the substrate is described through the Green's function formalism, while the mechanical fields in the electrodes are modeled using the finite-element method (FEM). The surface stress $\vec{T}$ and the surface charge σ present at the electrode-substrate interfaces act as sources of the wave fields.

3.3 Structure Characterization

In Paper I, the rigorous FEM/BEM simulator is employed to study leaky surface-acoustic waves (LSAW) on rotated Y-cut $LiNbO_3$ and $LiTaO_3$ substrates. These contain a weak but nonnegligible slow shear bulk-acoustic wave (SS-BAW) component, which results in the attenuation of the LSAW. The coupling is sensitive to frequency, the crystal cut angle, and the material and dimensions of the electrodes. Minimizing the losses of LSAW resonators is of considerable technical and economical importance. Significant reduction in the propagation loss on $LiTaO_3$ was achieved with the discovery [68, 69] that the coupling to the slow shear BAWs may be diminished by an optimal combination of the crystal cut angle and the thickness of the aluminum electrodes.

In Paper I, we have further studied the effect on $LiTaO_3$ and discovered similar optimal crystal orientations on $LiNbO_3$. In addition, it is demonstrated that the losses due to SS-BAW radiation may be suppressed by using very heavy electrodes. The phenomenon is illustrated in Fig. 3.2. In the test device with the heaviest electrodes, the resonance occurs at about 912.7 MHz. Since this is below the threshold frequency 916.1 MHz for synchronous BAW generation, the losses due to SS-BAW excitation are suppressed and the device features the best quality factor within the experiment.

Also shown are the simulations of the test devices, obtained with the FEM/BEM simulator and the infinite resonator model from Eq. (2.7). The predicted frequencies and quality factors of the resonances and antiresonances closely follow the experimentally observed tendencies. Most of the remaining discrepancies may be explained by the finite length and aperture, stray capacitances, and fabrication tolerances. The predicted losses close to the antiresonance are too small. Furthermore, the experiment with 9% electrode thickness also shows unknown ripples in the admittance above the resonance frequency. However, the comparison shows that the overall accuracy of the simulator is sufficient for qualitative and even quantitative structure characterization.

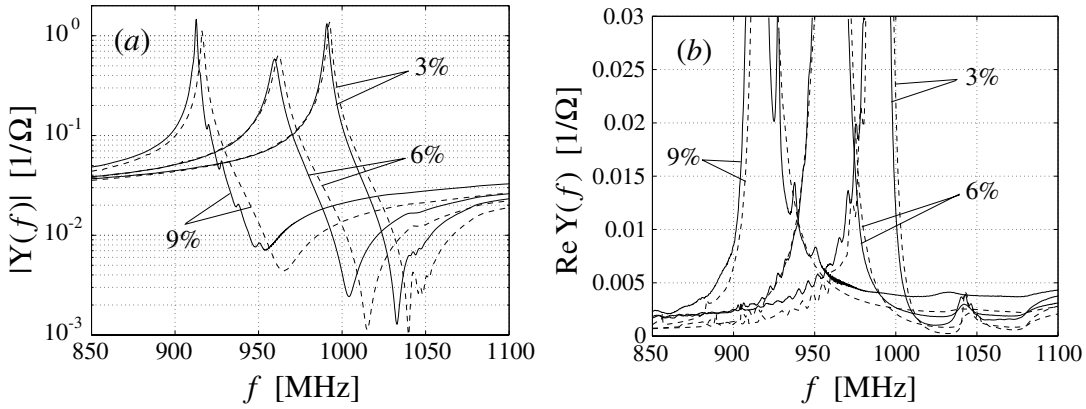

Figure 3.2: (a) Magnitude and (b) real part of the admittance for test structures with $h/2p = 3\%$, 6%, and 9% thick aluminum electrodes on 64°YX-cut $LiNbO_3$. Solid and dashed curves: experimental results and FEM/BEM simulations, respectively. Resistivity and attenuation have been introduced to the model phenomenologically.

Due to availability and price restrictions, simulations are often the only way to characterize new substrate crystals and orientations. For example, there has been much interest in the crystal langasite, see *e.g.*, Ref. [70]. The availability of the material is quite limited at the moment, but the materials parameters are known accurately enough for preliminary studies [71, 72]. In Paper II, the FEM/BEM simulator is applied to characterize surface transverse waves (STWs) on rotated Y-cut langasite. Based on the results, a temperature sensitivity similar to that in quartz and an electromechanical coupling coefficient several times higher than for STWs on ST-cut quartz is expected. However, in constrast to STW resonators on quartz, those on langasite appear to have excellent manufacturability.

3.4 Coupling-of-Modes Parameter Extraction

A particularly important and demanding form of the structure characterization is the extraction of the parameters used in phenomenological device models, such as the coupling-of-modes (COM) formalism [32]. The most straightforward theoretical approach is to deduce the parameters from the dispersion curves for shorted- and open-grating eigenmodes. In principle, the dispersion curves may be found directly by finding the poles and zeros of the harmonic admittance. However, in practice this is unattractive since the eigenmodes tend to have complex wavenumbers and the continuation of the harmonic admittance for complex-valued γ requires a cumbersome procedure [46].

In the procedure suggested by Zhang *et al.* [31] the contribution of the short-circuited eigenmodes to the harmonic admittance is decribed with a simple parametrized model. The dispersion curves are obtained indirectly by fitting the parametrized model to the rigorously computed harmonic admittance at each frequency of interest. Consequently, using a complex-valued γ is avoided. However, the method requires quite intensive computation and it is known [48] to run into difficulties for LSAWs when the surface-skimming bulk waves (SSBWs) contribute strongly to the harmonic admittance or interact with the LSAW [73].

In Paper III, we introduce a new procedure for the fast extraction of COM parameters from rigorous simulations for SAWs and LSAWs in birectional structures. In this approach, the harmonic admittance for $\gamma \approx 0.5$ is described within the COM formalism. The following expression, of the form of Eq. (2.9), may be derived:

$$\tilde{Y}_{\mathrm{COM}}\left(\gamma=\frac{1+q}{2}, f\right) = i\omega C_p \ \mathrm{sinc}(q) \frac{\bar{\Delta}_{\mathrm{oc}}^2(f)-q^2}{\bar{\Delta}_{\mathrm{sc}}^2(f)-q^2}, \quad |q| \approx 0. \tag{3.9}$$

Here, q measures the deviation of γ from the value 0.5, the capacitance per electrode pair C_p is a COM parameter, and $\bar{\Delta}_{\mathrm{oc}}$ and $\bar{\Delta}_{\mathrm{sc}}$ are normalized wavenumbers for eigenmodes of open-circuited and short-circuited electrode arrays, respectively. In the COM model, the dispersion relation for a short-circuited array is of the form

$$\bar{\Delta}_{\mathrm{sc}}(f) = \pm\sqrt{\left(f \cdot \frac{2p}{v} - 1 - i\frac{\gamma_a p}{\pi}\right)^2 - \left(\frac{|\kappa| p}{\pi}\right)^2}. \tag{3.10}$$

Here, v is wave velocity, the coupling coefficient κ measures reflectivity per unit length, and the parameter γ_a describes phenomenological attenuation. A similar result is obtained for an open-circuited grating but the parameters are weakly frequency dependent [42].

In unidirectional structures, the edges of the stopbands for shorted and open arrays are respectively manifested as two resonances and antiresonances in the admittance of an infinite transducer. Hence, the edges of the stopbands may be determined from the function $\tilde{Y}(0.5, f)$, see Ref. [74]. However, in bidirectional structures the stopbands for open and shorted gratings have one coinciding edge [75], such that one pole and one zero in the admittance cancel each other, and more information is required to determine the COM parameters.

In the extraction procedure described in Paper III, the frequency corresponding to the coinciding edge of the stopbands is located with a specially constructed phase-shift algorithm. From Eq. (3.9) it follows that, ignoring the sinc-factor, the dispersion relation may be expressed though the harmonic admittance as follows:

$$\bar{\Delta}^2_{\mathrm{sc}}(f) \approx q^2 \frac{\tilde{Y}(0.5(1+q), f) - i\omega C_p}{\tilde{Y}(0.5(1+q), f) - \tilde{Y}(0.5, f)}, \quad q \approx 0. \tag{3.11}$$

As in Zhang's algorithm, the extension of the harmonic admittance for complex-valued γ is avoided. Since the function needs to be evaluated for only two real values of γ at each frequency, the procedure is numerically very efficient. The price to pay is that the dispersion relation is constrained to the form of Eq. (3.10).

Since Eq. (3.9) is accurate within the COM formalism, the procedure also serves as a test for the validity of the COM theory. If the procedure fails, the model does not describe the structure with sufficient precision. For Rayleigh-type surface-acoustic waves in a narrow frequency range close to the stopband, the COM theory and Eq. (3.9) usually apply well. However, difficulties are encountered with LSAWs on rotated Y-cut $LiNbO_3$ and, in particular, $LiTaO_3$.

Owing to the interaction with fast-shear bulk-acoustic waves the LSAWs often feature strong dispersion, especially in the attenuation and the electromechanical coupling coefficient. The stronger the discrepancies between the COM model and the rigorous simulation, the harder it is to find an optimal set of parameters. In the phase-shift algorithm it is assumed that the parameters are constant and that the remaining admittance may be entirely described by a static capacitance. At frequencies below the threshold for FS-BAW generation, the algorithm usually works but the discrepancies between the simulation and the model slowly increase with frequency. The onset of the synchronous BAW radiation causes the phase-shift algorithm to utterly fail. Fortunately, for the electrode thicknesses $h/2p = 4 - 8\%$, currently used in RF SAW bandpass filters, this threshold has a sufficiently high frequency such that the edges of the stopbands may be determined.

The development of a phenomenological formalism more applicable to synchronous resonators employing LSAWs on rotated Y-cut $LiTaO_3$ is the topic of Paper IV, discussed in Sec. 4.

4 Model for Shear Horizontal Waves

The coupling-of-modes model has been remarkably successful in describing devices based on conventional Rayleigh-type surface acoustic waves, substantially slower than bulk-acoustic waves and with mainly sagittal polarization. However, the model is considerably less adequate for dominantly shear horizontal surface-acoustic waves (SH-SAWs), such as surface transverse waves (STWs), and leaky surface-acoustic waves (LSAWs) on rotated Y-cut $LiNbO_3$ and $LiTaO_3$.

Approaches to describe shear-horizontal waves typically consider STW propagation in a periodic grating on a quartz substrate and utilize the Floquet expansion and approximate boundary conditions such as the Datta-Hunsinger boundary conditions [76], see, *e.g.*, Refs. [77, 78]. Danicki [79] derived a phenomenological model for the harmonic admittance. The characteristics of the SH-SAW propagation in a periodic grating are well described by a phenomenological model due to Plessky [80], reviewed below. In Paper IV we have extended Plessky's dispersion model for the excitation of SH-SAWs in finite electrode structures, thus obtaining a model for synchronous SH-SAW resonators.

4.1 Propagation in the Periodic Electric Array

A characteristic of shear horizontal surface-acoustic waves is that their velocity is close to that of fast shear bulk-acoustic waves (FS-BAWs). SH-SAWs may be interpreted as FS-BAWs localized to the surface by some physical mechanism, such as an interaction with the electric fields in piezoelectric substrates (Bleustein-Gulyaev waves [81], LSAWs in $LiNbO_3$ [82] and $LiTaO_3$ [83]), mass loading (Love waves [84]), or loading by periodic electrode structures (STWs [85,86]). The localization depth of the SH-SAW is determined by the small difference in the velocities of the surface and bulk waves, and (in contrast to Rayleigh waves) it strongly depends on the strength of the surface perturbation. In devices employing SH-SAWs this may result in strong dispersion and scattering into FS-BAWs, sometimes called SAW-BAW interactions, and in a parasitic excitation of the FS-BAWs.

Consider the structure in Fig. 2.1. In Plessky's dispersion model [80] the SH-SAW eigenmodes of the periodic grating are sought within the coupling-of-modes approximation, in the form

$$u(x,z) = u_+ e^{-i\gamma Q x} e^{K_+ z} + u_- e^{-i(\gamma-1)Qx} e^{K_- z}. \tag{4.1}$$

Here, the definitions are as in Fig. 2.1, and u_+ and u_- represent the amplitudes of the incident and reflected waves, respectively, $Q = 2\pi/p$ is the grating wavenumber, and $\gamma = (1+q)/2$ is the normalized wavenumber of the incident wave. The factors

$K_\pm$ describe the localization of the wave to the surface:

$$K_\pm = \sqrt{\left(\frac{Q}{2}\right)^2 (1 \pm q)^2 - k_\mathrm{B}^2}. \tag{4.2}$$

Here, $k_\mathrm{B} = \omega/v_\mathrm{B}$ and v_B denotes the velocity of the FS-BAW. The BAW slowness curves is assumed isotropic in the xz-plane. The cut line for the square root in Eq. (4.2) is chosen such that the surface-type waves decay and the bulk-type waves propagate as $z \to -\infty$.

For Bleustein-Gulyaev waves propagating on a metallized surface with a periodic mass density, boundary conditions in the form

$$\begin{cases} \left(K_+ - \eta_0 \dfrac{Q}{2}(1+q) - 2\varepsilon_0 \dfrac{k_\mathrm{B}^2}{Q}\right) u_+ = 2\varepsilon_1 \dfrac{k_\mathrm{B}^2}{Q}\, u_-, \\ \left(K_- - \eta_0 \dfrac{Q}{2}(1-q) - 2\varepsilon_0 \dfrac{k_\mathrm{B}^2}{Q}\right) u_- = 2\varepsilon_1^* \dfrac{k_\mathrm{B}^2}{Q}\, u_+. \end{cases} \tag{4.3}$$

may be derived [87]. Here, η_0 is the piezoelectric coupling constant and the parameters ε_0 and ε_1 describe the uniform mass loading and the coupling between the counter-propagating waves, respectively. The dispersion equation is obtained by setting the determinant

$$D(\gamma, f) = \left(K_+ - \eta_0 \gamma Q - 2\varepsilon_0 \frac{k_\mathrm{B}^2}{Q}\right)\left(K_- - \eta_0 (1-\gamma) Q - 2\varepsilon_0 \frac{k_\mathrm{B}^2}{Q}\right) - 4|\varepsilon_1|^2 \frac{k_\mathrm{B}^4}{Q^2} \tag{4.4}$$

to vanish. An approximate solution in closed form is derived in Ref. [80]. The exact solution may be found by converting the dispersion equation into a quartic polynomial and finding the roots of the polynomial. Hence, the dispersion is in principle available in closed form but, owing to the length of the resulting expressions, the exact approach is practical for numerical evaluation only.

With the periodic load interpreted as an effective description of an electrode array, the dispersion relation obtained serves as a model for the SH-SAW propagation in a periodic grating, see Fig. 4.1. For frequencies far below the bulk-wave threshold $f_\mathrm{B} = v_\mathrm{B}/2p$ the eigenmode characteristics are similar to those of Rayleigh-type surface-acoustic waves in periodic gratings. However, the localization depth of the wave grows ($K_\pm$ decrease) with increasing frequency until the reflected wave becomes entirely delocalized: it is converted into a bulk wave and radiated into the substrate. This scattering of the SH-SAW into BAWs results in pronounced attenuation of the incident wave and, as illustrated in Fig. 4.1, it may cause a premature collapse of the stopband.

For LSAWs in $LiNbO_3$, the localization depth is determined by the high piezo-coupling and the stopband is well separated from frequency region with bulk-wave generation. However, for LSAWs in $LiTaO_3$ the upper edge of the stopband may extend close to the bulk-wave threshold, and for STWs in quartz it may even exceed it. Consequently, even small changes in the velocity inside the stopband result in a strong change of the localization depth.

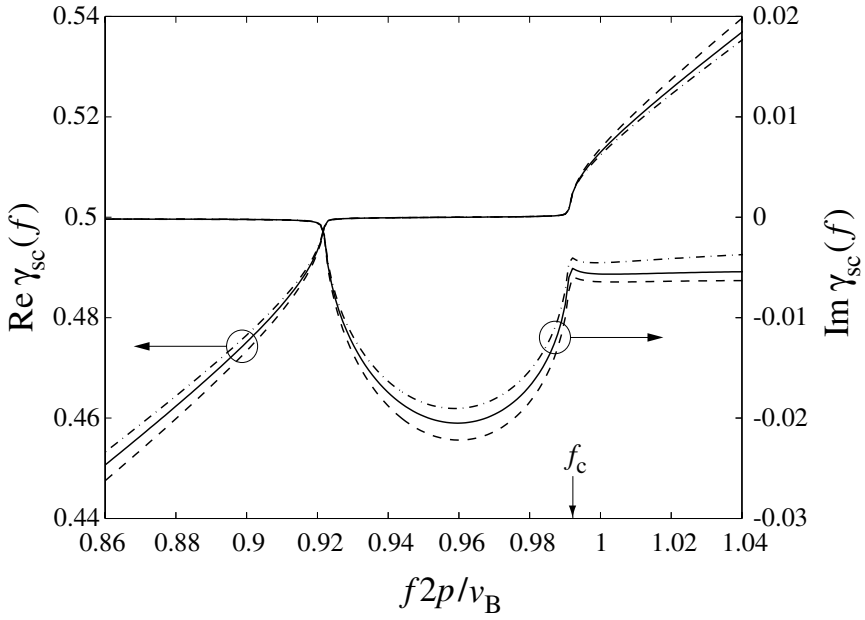

Figure 4.1: Dispersion curves for SH-SAWs in periodic gratings as functions of the normalized frequency, with parameters determined to yield coinciding edges of the stopband. Scattering into BAWs begins at the frequency f_c and causes a collapse of the stopband. Solid curves: η_0=0.269, ε_0=0, and ε_1=0.139. Dashed curves: η_0=0, ε_0=0.295, and ε_1=0.161. Dash-dotted curves: the approximate solution from Ref. [80].

4.2 Abbott-Hashimoto Coupling-of-Modes Model

Abbott and Hashimoto succeeded in combining the approximate closed-form dispersion relation with the COM framework [88, 89]. Their construction is brilliant in that the COM formalism, providing closed-form formulas for the components of the P-matrix, may be used and, simultaneously, the SH-SAW dispersion characteristics are adequately described. However, a few problems remain not solved.

The approximate dispersion relation treats the unperturbed waves as surface-skimming bulk waves (SSBW). This approximation holds only if the piezoelectric coupling and uniform loading remain small. Near the stopband the localization depth is determined by the Bragg reflections, but for large frequency detunings even a weak uniform load may localize the SSBW. This causes a minor but systematic error in the velocity, see Fig. 4.1. The discrepancy has been verified based on numerical simulations, and a correction constant to be included into the theory has been suggested [89, 90].

Due to changes in the localization of the counterpropagating components of the eigenmodes as functions of frequency, the normalization of the wave amplitudes is difficult. The direct excitation of bulk-acoustic waves is entirely ignored. Consequencely, the description of the electromechanical coupling is unsatisfactory [89, 91, 92].

Finally, although the theory describes the scattering of the SH-SAW into bulk waves in a periodic grating, the additional mode conversion occurring at discontinuities, such as gaps [90] and the edges of the structure, is not taken into account. The mode conversion is especially strong for STWs since the structure of the wave inside the electrode grating and on a free or metallized surface can be considerably different—sometimes a STW does not even exist on a free surface.

4.3 Phenomenological Resonator Model

In Paper IV, we have constructed a phenomenological model for synchronous resonators employing SH-SAWs. The approach is based on extending Plessky's dispersion model for the excitation of SH-SAWs in finite electrode structures. With somewhat higher computational cost, it inherently copes with most of the difficulties discussed above.

The principal constituents of the theory are the phenomenological scalar Green's function $G(x)$, which relates the scalar displacement field on the surface $u(x)$ to the scalar surface stress field $T(x)$ via

$$u(x) = \int_{-\infty}^{+\infty} G(x - x')T(x')dx', \tag{4.5}$$

and the phenomenological boundary condition

$$T(x) = \rho h(x)\,\omega^2 u(x) + S(x). \tag{4.6}$$

Here, $\rho h(x)$ is effective mass density on the surface while $S(x)$ is a source term, responsible for the excitation of the acoustic fields. Consistency with Eq. (4.3) requires a Green's function of the form

$$\tilde{G}(\beta) = \left[\sqrt{\beta^2 - k_{\mathrm{B}}^2} - \eta_0\beta^{(+)}\right]^{-1}, \tag{4.7}$$

and an effective mass density

$$\rho h(x) = \frac{2}{Qv_{\mathrm{B}}^2}\Big(\varepsilon_0 + 2|\varepsilon_1|\cos(Qx+\theta_{\mathrm{r}})\Big)\,\Theta\left(Np-2|x|\right). \tag{4.8}$$

Above, $\beta^{(+)}$ denotes $\pm\beta$ with the sign of the real part chosen positive and θ_{r} is the phase of the parameter ε_1; the phase determines the location of the reflectivity center inside each period. $\Theta(x)$ is the Heaviside step function and N is the number of periods in the array.

In the limit of an infinite grating ($N\to\infty$), full equivalence with Plessky's model is obtained by omitting the source term $S(x)$. To describe electric excitation and current generation, a finite source term is allowed and acoustic currents proportional to the displacement at the electrode centers are assumed. Introducing an excitation term of the harmonic form, an analytic model for the harmonic admittance may be obtained:

$$\tilde{Y}_{\mathrm{SH}}(\gamma, f) = i\omega C(\gamma)\frac{D_{\mathrm{oc}}(\gamma, f)}{D_{\mathrm{sc}}(\gamma, f)}. \tag{4.9}$$

Here, the function $C(\gamma)$ describes the slowly varying capacitive contribution to the harmonic admittance while the dispersion functions D_{oc} and D_{sc} are of the form of Eq. (4.4). The dispersion equations for open-circuited and short-circuited arrays are obtained by setting the respective dispersion functions equal to zero.

A model for a finite synchronous resonator is obtained by limiting the excitation to N_{p} electrode pairs and by setting $N = 2(N_{\mathrm{g}} + N_{\mathrm{p}})$, where N_{g} is the number of electrodes in each reflector, see Fig. 4.2. This results in an integral equation for the surface stress; a rather similar method has been used earlier by Rønnekleiv [93]. With complex-analytic techniques, the solution is found to consist of the solution for the corresponding infinite one-port resonator and of terms describing the reflections and mode conversion occuring at the reflector edges. Evaluating the reflected bulk-acoustic waves with the steepest descent method, approximate surface stress in algebraic form is found.

The result in Eq. (4.9) allows the extraction of the parameters of the theory from rigorous FEM/BEM simulations. The determination of the parameter η_0 is somewhat contradictory: besides influencing the eigenmodes inside a grating, it also describes the SH-SAW characteristics outside the structure (typically, on free or metallized crystal surface). Consequently, it should also reflect the mode conversion occurring at the edges of a finite structure. According to this reasoning, two separate parameters η_0 should be incorporated into the model: one in the Green's function to describe the surface outside the device, the other one in the boundary condition to describe the grating—but this has not been done within this work.

A fit of the model in Eq. (4.9) to rigorous computed harmonic admittance on 42°YX-cut $LiTaO_3$ is displayed in Fig. 4.3(a). A satisfactory quantitative agreement is reached, although some discrepancies may also be observed. Since the wave on this cut is not entirely SH-SAW but LSAW, the model overestimates the radiation of fast-shear bulk-acoustic waves at frequencies close to and above the threshold f_{B}. The excitation of slow shear bulk-acoustic waves, responsible for the losses at lower frequencies and clearly nonnegligible in the stopband frequencies, is not fully covered by the model. As a consequence, the predicted antiresonance and the peak at the upper edge of the stopband are far too sharp.

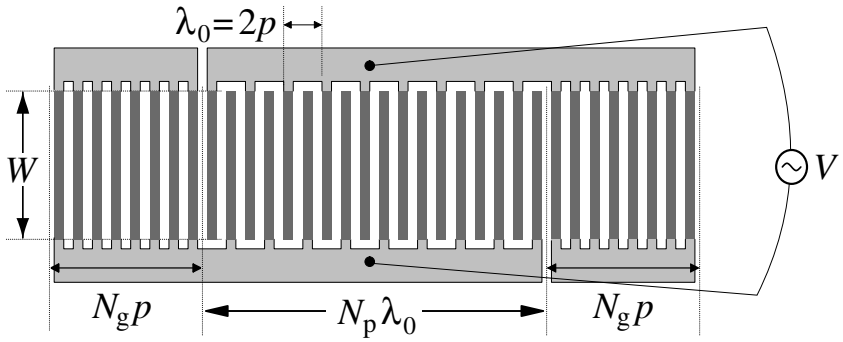

Figure 4.2: Schematical synchronous resonator.

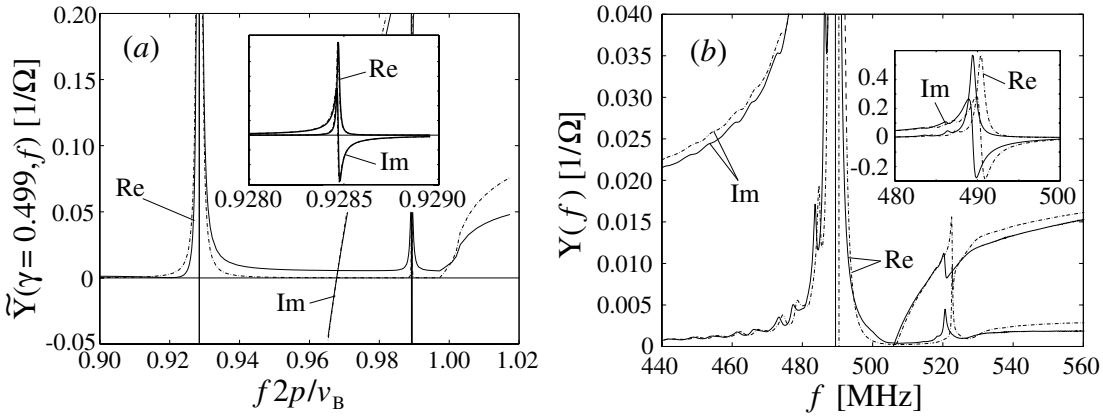

Figure 4.3: Comparison of the model (*dashed curves*) to (*solid curves*:) (a) the harmonic admittance $\tilde{Y}(0.499, f)$ and (b) the measured response of a test resonator. Here, h/λ_0=8%, a/p=0.6, and the substrate is 42°YX-cut $LiTaO_3$. In the test resonator $p = 4$ μm, N_p=75, N_g=37 and W=16λ_0.

A simulated resonator response is compared to a test structure measurement [94] in Fig. 4.3(b). Phenomenological attenuation, a series resistance of 1.4 Ω, and some additional capacitance were introduced to the model, but otherwise the parameters are those deduced from the FEM/BEM simulation. The resonance frequency is slightly shifted and there is small error in the dispersion characteristics. These effects may be explained by waveguiding and deviations in the device geometry. However, the achieved overall accuracy exceeds that of conventional COM theory, especially concerning the shape of the resonance. As expected based on Fig. 4.3(a), the predicted losses at the stopband are somewhat too low and the BAW radiation at high frequencies is overestimated. However, the experimental curve also features an unexpected increase in the conductance in the r.h.s. of the resonance. The mechanism underlying the related losses—LSAW radiation to the busbars of the resonator—is the topic of Papers V and VI, discussed in Sec. 5.

5 Acoustic Losses in Leaky SAW Resonators on $LiTaO_3$

Leaky surface-acoustic wave resonators on rotated Y-cut $LiTaO_3$ substrates feature strongly frequency-dependent losses, as can been seen in Fig. 4.3. These lead to deterioration in the filter performance and require corrections in device design [95]. Although the contributions of phenomena such as the backscattering into FS-BAWs and the synchronous BAW excitation to the losses have been studied [73], the leakage mechanisms in LSAW resonators have remained weakly understood.

Recently, laser-interferometric measurements by Knuuttila *et al.* revealed that acoustic waves are capable of escaping the resonator area through the busbars [96,97]. In Paper V of this work, the escaping acoustic beams have been identified as LSAW radiation and their characteristic features have been qualitatively explained based on the crystalline anisotropy of the lithium tantalate substrate. Furthermore, in Paper VI we have quantitatively analyzed the frequency-dependence of the radiation and estimated the acoustic losses due to the effect as well as those due to LSAW propagation losses, LSAW backscattering into FS-BAWs, and the FS-BAW excitation. The analysis is based on the infinite periodic grating with a finite aperture, illustrated in Fig. 5.1.

Due to the high anisotropy of the LSAW slowness curves on rotated Y-cut $LiTaO_3$ substrates, conventional scalar waveguide theories based, for example, on the paraxial approximation [38] are unsuitable for LSAW devices. In Paper VI, a semi-phenomenological, semi-empirical model is constructed for the harmonic admittance of the infinite electrode array with a finite aperture. The model may be considered as a two-dimensional extension of the SH-SAW resonator model in Paper IV. An algebraic Green's function $G(x, y)$ is empirically constructed such that the slowness curves for LSAWs under uniform metallization on $LiTaO_3$ are reproduced by theory with a reasonable accuracy. The excitation of fast-shear BAWs is inherently included, but

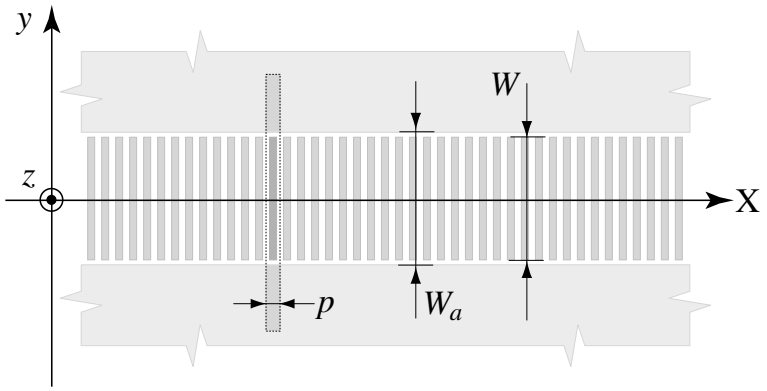

Figure 5.1: Periodic electrode array with infinite busbars.

the slow-shear BAW contribution is accounted for only in the propagation loss of the LSAW. Solving the model numerically and applying the analysis techniques reviewed in Sec. 2, the displacement fields and the electric admittance in an infinite resonator may be computed, enabling quantitative analysis of the leakage mechanisms.

5.1 Acoustic Leakage Mechanisms

Laser-interferometric scans of the acoustic field in synchronous resonators on 36°YX-$LiTaO_3$ reveal strongly frequency-dependent acoustic radiation to the busbars of the structure, as shown by the series of images in Fig. 5.2. In Paper V the phenomenon is qualitatively explained based on the slowness curves and the polarization for LSAWs on uniformly metallized $LiTaO_3$ surface.

In the stopband the acoustic field in the grating area is governed by the Bragg reflections. At certain frequencies the busbars (which may be considered as metallized crystal surface) support LSAW eigenmodes which are synchronously coupled to the acoustic field in the grating. Leaky waveguide modes have been studied earlier on 112°-$LiTaO_3$ [98] and on ST-cut quartz [99, 100]. A detailed analysis of mass-loaded slowness curves in Paper VI confirms that the predicted frequency-dependence of the radiation closely matches both with the laser-interferometric scans and with the electrical measurements. Furthermore, the frequencies most prone to the radiation depend only on the relative metallization thickness.

Due to the anisotropy of the substrate crystal, the detected radiation is spatially asymmetric. Although the LSAW slowness curves are symmetric about the crystal X-axis, the polarization is not. The asymmetry is particularly strong for the weak shear vertical component which the interferometer detects. Indeed, measurements have confirmed that the favoured direction of the radiation is independent of the polarity of the electric drive. However, according to our computations the dominant shear horizontal component is almost symmetric. This suggests that, despite the probe images, LSAWs are actually radiated to the busbars almost symmetrically.

Figure 5.3 illustrates the simulated displacement profiles obtained from the infinite resonator model in Paper VI. In constrast to the laser-interferometric scans measuring the shear vertical component, the scalar displacement field treated by the model is interpreted to describe the dominant shear horizontal component and it is assumed symmetric. Due to the finite size of the test resonator, differences are seen in the leakage through the reflectors. However, a close similarity is observed between the measured and modeled amplitude distributions and, in particular, in the radiation leaking to the busbars.

In addition to LSAWs, also Rayleigh waves may be radiated synchronously to the busbars. Both synchronous and transversally excited Rayleigh waves are observed in the laser-interferometric scans reported in Paper VI, but they are likely to be rather weak. Other acoustic leakage mechanisms include the radiation of bulk-acoustic waves, which are interpreted to yield the weak acoustic background visible in the scans.

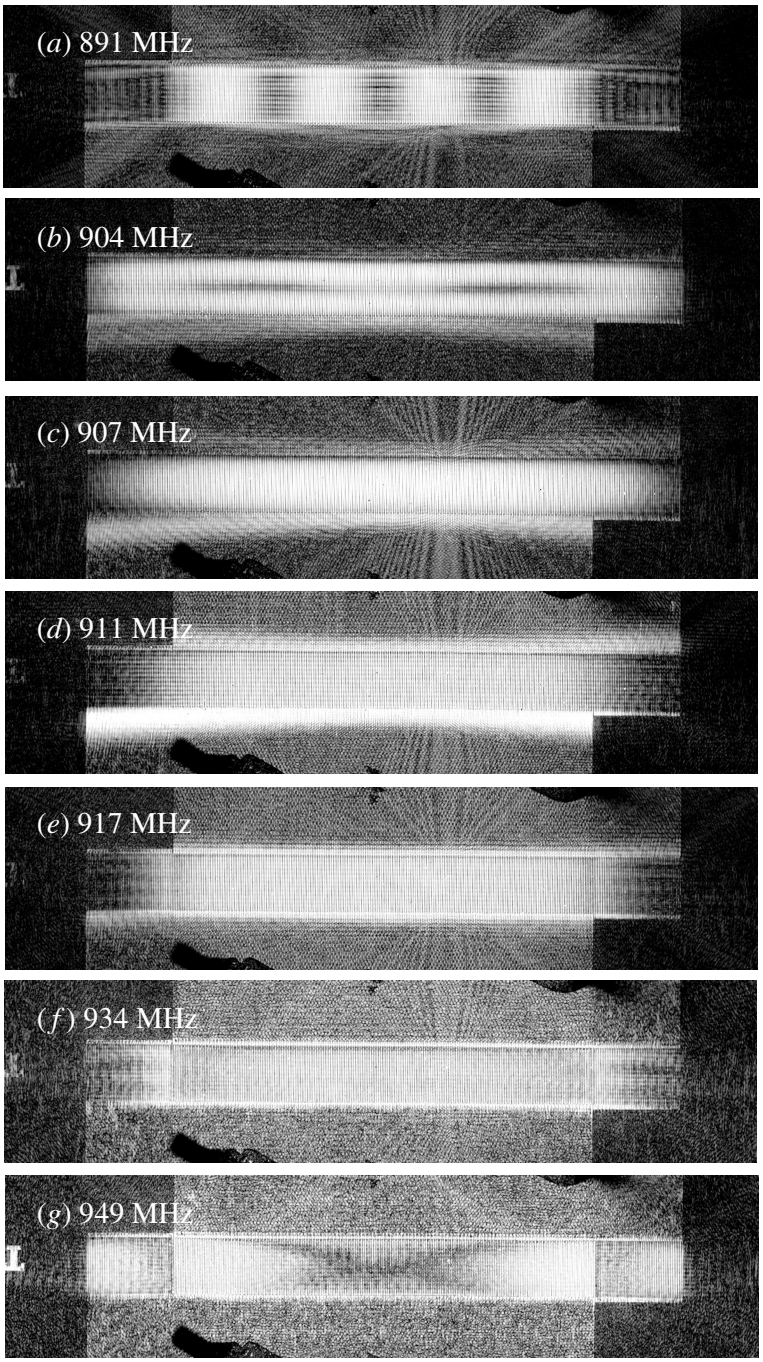

Figure 5.2: Experimental shear vertical displacement profiles measured with a laser probe, featuring LSAW radiation to the busbars in a test resonator on 36°YX-cut $LiTaO_3$. Below the resonance frequency (a, b) the radiation is weak, but strong radiation occurs slightly above the resonance (c, d). Towards a quenching frequency of about 917 MHz the radiation diminishes (e) and virtually disappears (f, g). The displacement in the metallized and free crystal surfaces are not in scale. *Courtesy of Jouni Knuuttila.*

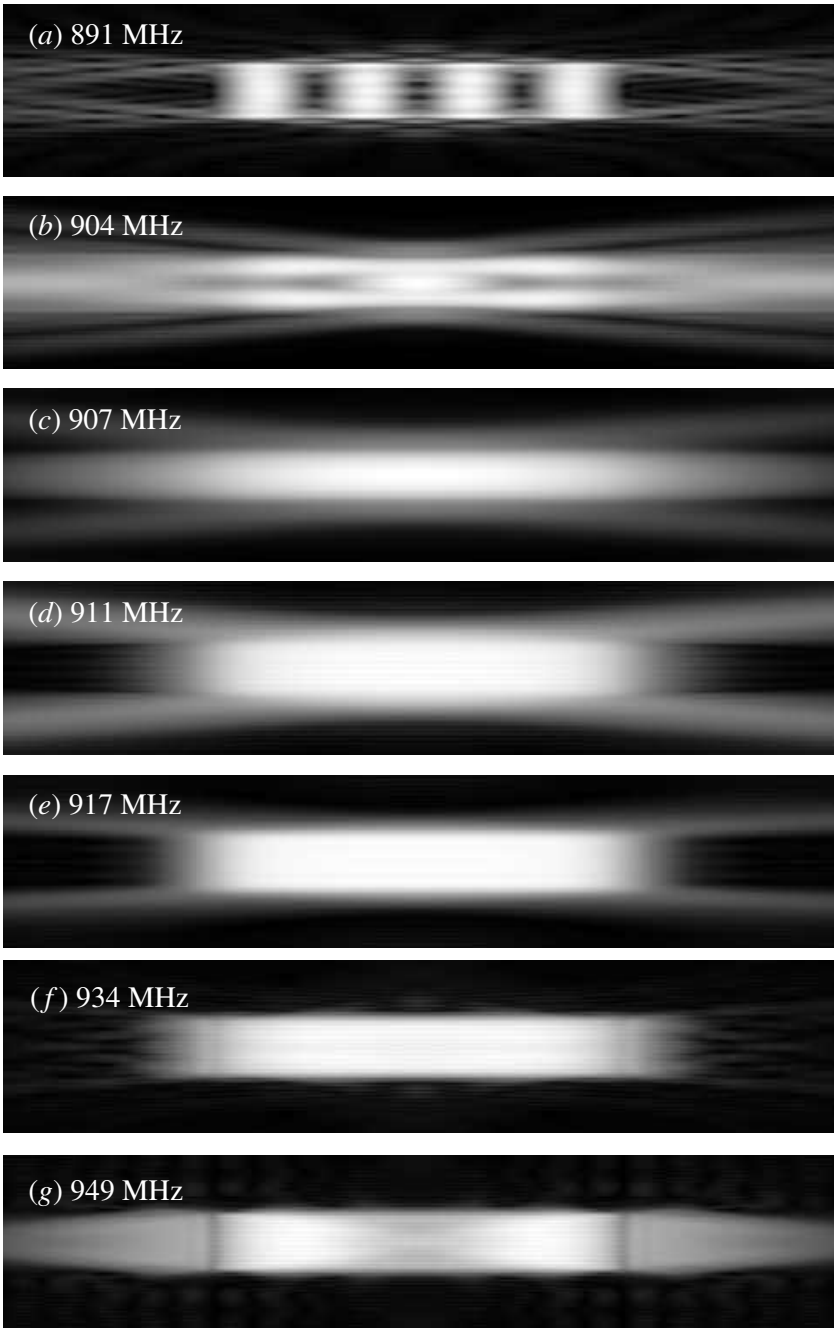

Figure 5.3: Simulated shear horizontal displacement profiles for the test structure of Fig. 5.2, obtained with a phenomenological model for infinite resonators.

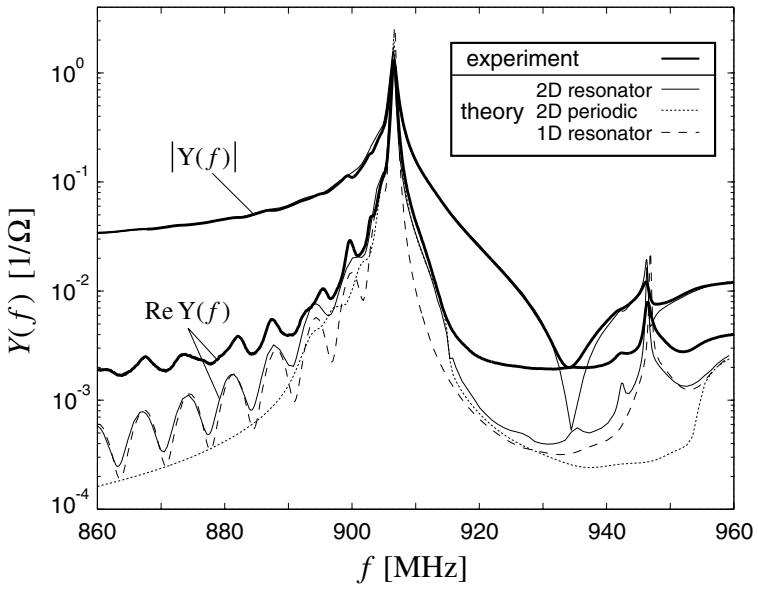

Figure 5.4: Measured and simulated admittance and conductance of the test structure in Figs. 5.2 and 5.3. For a reference, also the simulations for an infinite transducer and a resonator with an effectively infinite aperture are shown.

5.2 Leakage and the Electric Performance

The model also allows us also to estimate the effect of the acoustic radiation on the electric response of the resonator. Simulations confirm that the LSAW busbar radiation is indeed responsible for the experimentally observed increase in the conductance in the vicinity of the resonance, see Fig. 5.4. Further experiments and simulations in Paper VI indicate that the strength of the radiation depends only weakly on the acoustic aperture. Consequently, the relative losses are pronounced for narrow apertures.

An interesting feature of the scanned images and the simulations is the almost total absence of transversal resonances. In Paper VI, this is attributed to the fact that, for both 36° and 42°cut $LiTaO_3$, the LSAW attenuation increases drastically with the propagation angle off the crystal X-axis. Consequently, higher order transversal waveguide modes are likely to display strong propagation losses.

According to the simulations, the busbar radiation and the LSAW attenuation well explain the losses close to and slightly above the resonance. These may also be responsible for the very high values of series resistance required in the SH-SAW resonator model (Paper IV). At high frequencies, the excitation of the fast shear bulk-acoustic waves is the dominating loss mechanism. However, these effects cannot explain the experimentally observed losses in the stopband and, in particular, in the vicinity of the antiresonance. These may be due to the direct excitation of the slow shear bulk-acoustic waves and the acoustic losses in the electrodes. More research is required on this aspect, as well as to find the means to optimize the resonator to minimize the losses.

6 Discussion and Conclusions

This dissertation is concerned with the analysis and simulation of surface-acoustic waves. The carrying theoretical concept is the excitation of acoustic waves in a period electrode array. This so-called excitation problem proves appropriate for computer simulations with both rigorous and phenomenological approaches. The resulting resonance phenomena are characteristic to the considered structures and they enable comparisons with experimental measurements and other theories. The treatment may be extended to synchronous uniform resonators by taking into consideration the acoustic reflections occuring at the edges of the structure. The main results of this work are summarized below as concluding remarks.

Structure characterization based on rigorous simulation of periodic electrode arrays with infinite aperture

The properties of resonating SAW devices depend crucially on the choice of the piezoelectric substrate material, crystal cut, and the width, height and shape of the electrodes. In this work we have implemented a periodic structure simulator and demonstrated that it yields quantitative information on the resonator performance, including the resonance and antiresonances frequencies and losses due to bulk-wave radiation, with a precision that enables the identification of optimal crystal orientations and structures. The simulator has been applied to analyze, in detail, SH-SAWs on rotated Y-cut $LiNbO_3$, $LiTaO_3$, and langasite substrates.

Coupling-of-modes parameter extraction

The extraction of parameters used in phenomenological models, such as the coupling-of-modes formalism, may be seen as one particular form of structure characterization. It has been shown here that the coupling-of-modes parameters for uniform electrode structures may be determined theoretically from the rigorously computed harmonic admittance of a periodic electrode array using a new, efficient phase-shift algorithm.

Model for shear horizontal surface-acoustic wave resonators

In this work, Plessky's dispersion model for shear horizontal waves has been extended to wave excitation in finite and periodic electrode structures, resulting in a model for synchronous one-port resonators. The model is compared with rigorous numerical simulations of periodic structures and electrical measurements from test devices. Excellent agreement is found on the dispersion characteristics and the shape of the resonance, while some of the losses at the stopband frequencies remain unexplained and require more detailed treatment or further investigation. The accuracy achieved exceeds those of coupling-of-modes models. With the parametrization resembling that in COM—while the

computational requirements are only modestly higher than those for COM—the new model has strong potential for replacing COM as the design tool for the synthesis of impedance element filters.

Analysis of acoustic losses in leaky surface-acoustic wave resonators with finite aperture on lithium tantalate

Within this work, various theoretical methods, including a new phenomenological periodic waveguide model, have been employed to study the acoustic loss mechanisms observed in leaky surface-acoustic wave resonators on rotated Y-cut lithium tantalate substrates. In particular, it has been shown that the radiation of LSAWs into the busbars of the resonator well explains the asymmetric radiation observed with laser-interferometric scans of the device and the increased losses visible in the electrical measurements close to the resonance. The importance of the propagation losses to the suppression of high-order transversal modes is also recognized. Minimizing the waveguide losses poses a future challenge with considerable technological importance.

There is an evident need for improved simulation software in the SAW industry. Precise design models reduce the number of design cycles and help to improve the manufacturing yield. Furthermore, the development of mobile telecommunication applications towards higher operation frequencies requires new substrate materials and crystal cuts with high wave velocities and low fabrication sensitivites. Physical simulators may be used to identify promising substrate and structure candidates for experimental inspection. With the recent drastic pace of increase in the computational resources it is easy to envision ever more accurate and comprehensive models.

Rigorous simulators for devices with a finite number of electrodes have been reported and are being actively implemented [56, 101, 102]. However, it should be remembered that even the precision of such sophisticated tools may not be enough for device design. Rigorous models suffer from uncertainties in the electrode shape, material parameters, wafer quality, and wafer homogeneity. Most important of all, as demonstrated also in this work, the effects related to the finite aperture of real components may significantly distort the device response. For this reason it is interesting to see whether field-theoretical models capable of describing finite apertures will appear within a few years. Since such a simulation is a colossal task, the periodic electrode array again appears as an attractive route to the analysis.

Another interesting question is the impact of the increased computational capacity on phenomenological models. Evidently, the design tools would highly benefit from the proper description of the peculiarities of shear-horizontal surface waves and the waveguide phenomena. The difficulty in the development of phenomenological models lies in the absence of a systematic theory. Whether the concepts introduced in the present work will evolve into practical design models or if another, improved approaches will be found, remains to be seen.

References

[1] Lord Rayleigh,"On waves propagated along the plane surface of elastic solid", *Proc. London Math. Society* **17**, 4-11 (1885).

[2] J. Curie and P. Curie,"Développement, par pression, de l'électricité polaire dans les cristaux hémièdres à faces inclinées", *Bull. Soc. Min. de France* **3**, 90-93 (1880).

[3] R. M. White and F. W. Voltmer, "Direct piezoelectric coupling to surface elastic waves", *Appl. Phys. Lett.* **7**, 314-316 (1965).

[4] D. P. Morgan, *Surface-Wave Devices for Digital Signal Processing* (Elsevier, 1991).

[5] E. Ash, "Surface wave grating reflectors and resonators", *Digest of IEEE Microwave Theory and Techniques Symp.* (1970), pp. 385-386.

[6] W. Tanski, "Surface-acoustic wave resonators on quartz", *IEEE Trans. Sonics Ultrason.* **26**, 93-104 (1979).

[7] P. S. Cross, W. R. Schreve, and T. S. Tan, "Synchronous IDT SAW resonators with Q above 10000", in *Proc. 1979 IEEE Ultrason. Symp.*, pp. 824-829.

[8] P. S. Cross, R. V. Schmidt, "Coupled surface-acoustic-wave resonators", *The Bell system technical journal*, 1447-1482 (1977).

[9] P. V. Wright, "A review of SAW resonator filter technology", in *Proc. 1992 IEEE Ultrason. Symp.*, pp. 29-38.

[10] G. K. Montress, T. E. Parker, and D. Andres, "Review of SAW oscillator performance", in *Proc. 1994 IEEE Ultrason. Symp.*, pp. 43-54.

[11] G. S. Kino, S. Ludvik, H. J. Shaw, W. R. Shreve, J. M. White, and D. K. Winslow, "Signal processing by parametric interactions in delay-line devices", *IEEE Trans. Microwave Theory and Tech.* **21**, 244-255 (1973).

[12] M. Luukkala and G. S. Kino, "Convolution and time inversion using parametric interactions of acoustic surface waves", *Appl. Phys. Lett.* **18**, 393-394 (1971).

[13] D. S. Ballantine, R. M. White, S. I. Martin, A. I. Ricco, E. T. Zellers, G. C. Frye, and H. Wohltjen, *Acoustic Wave Sensors* (Academic Press, 1997).

[14] V. P. Plessky, S. N. Kondratiev, R. Stierlin, and F. Nyffeler, "SAW tags: new ideas", in *Proc. 1995 IEEE Ultrason. Symp.*, pp. 117-120.

[15] O. Ikata, T. Miyashita, T. Matsuda, T. Nishihara, and Y. Satoh, "Development of low-loss band-pass filters using SAW resonators for portable telephones", in *Proc. 1992 IEEE Ultrason. Symp.*, pp. 111-115.

[16] O. Ikata, Y. Satoh, H. Uchishiba, H. Taniguchi, N. Hirasawa, K. Hashimoto, and H. Ohmori, "Development of small antenna duplexer using SAW filters for handheld phones", in *Proc. 1993 IEEE Ultrason. Symp.*, pp. 111-114.

[17] M. Hikita, N. Shibagaki, T. Akagi, and K. Sakiyama, "Design methodology and synthesis techniques for ladder-type SAW resonator coupled filters", in *Proc. 1993 IEEE Ultrason. Symp.*, pp. 15-24.

[18] M. Ueda, O. Kawachi, K. Hashimoto, O. Ikata, and Y. Satoh, "Low loss ladder type SAW filter in the range of 300 to 400 MHz", in *Proc. 1994 IEEE Ultrason. Symp.*, pp. 143-146.

[19] J. Heighway, S. N. Kondratiev, and V. P. Plessky, "Balanced bridge SAW impedance element filters", in *Proc. 1994 IEEE Ultrason. Symp.*, pp. 27-30.

[20] T. Morita, Y. Watanabe, M. Tanaka, and Y. Nakazawa, "Wideband low loss double mode SAW filters", in *Proc. 1992 IEEE Ultrason. Symp.*, pp. 95-104.

[21] M. A. Sharif, C. Lambert, D. P. Chen, and C. S. Hartmann, "Network coupled, high performance SAW resonator filters", in *Proc. 1994 IEEE Ultrason. Symp.*, pp. 135-138.

[22] European Patent Application EP0845858A2, 1998, FUJITSU LIMITED; M. Ueda, O. Kawachi, G. Endoh, and Y. Fujiwara, "Surface acoustic wave device".

[23] H. F. Tiersten and R. C. Smythe, "Guided acoustic surface wave filters", in *Proc. 1975 IEEE Ultrason. Symp.*, pp. 293-294.

[24] M. Tanaka, T. Morita, K. Ono, and Y. Nakazawa, "Narrow bandpass filters using double-mode SAW resonators on quartz", in *Proc. 38th Freq. Contr. Symp.* (1980), pp. 286-293.

[25] G. Martin, "Transversely coupled resonator filters", in *Proc. 1999 IEEE Ultrason. Symp.*, pp. 15-24.

[26] M. Lewis, "SAW filters employing interdigitated interdigital transducers", in *Proc. 1982 IEEE Ultrasonics Symposium*, pp. 12-17.

[27] M. Hikita, T. Tabuchi, H. Kojima, A. Nakagoshi, and Y. Kinoshita, "Low loss filter for antenna duplexer", in *Proc. 1983 IEEEE Ultrasonics Symposium*, pp. 77-82.

[28] V. P. Plessky, "SAW design bridges technology gap", *RF Design*, 46-54 (1998).

[29] K. Bløtekjær, K. A. Ingebrigtsen and H. Skeie, "A method for analyzing waves in structures consisting of metal strips on dispersive media", *IEEE Trans. Electron Devices* **20**, 1133-1138 (1973).

[30] K. Bløtekjær, K. A. Ingebrigtsen and H. Skeie, "Acoustic surface waves in piezoelectric materials with periodic metal strips on the surface", *IEEE Trans. Electron Devices* **20**, 1139-1146 (1973).

[31] Y. Zhang, J. Desbois, and L. Boyer, "Characteristic parameters of surface acoustic waves in a periodic metal grating on a piezoelectric substrate", *IEEE Trans. Ultrason., Ferroelect., Freq. Contr.* **40**, 183-192 (1993).

[32] P. V. Wright, "A new generalized modeling of SAW transducers and gratings", in *Proc. 43th Freq. Contr. Symp.* (1989), pp. 596-605.

[33] G. Tobolka, "Mixed matrix representation of SAW transducers", *IEEE Trans. Sonics Ultrason.* **26**, 426-428 (1979).

[34] C. C. W. Ruppel, W. Ruile, G. Scholl, K. Ch. Wagner, and O. Männer, "Review of models for low-Loss filter design and applications", in *Proc. 1994 IEEE Ultrason. Symp.*, pp. 313-324.

[35] C. Elachi, "Waves in active and passive periodic structures: a review", *Proc. of the IEEE* **64**, 1666-1698 (1976).

[36] H. A. Haus and W. Huang, "Coupled-mode theory", *Proc. of the IEEE* **79**, 1505-1518 (1991).

[37] Y. Suzuki, H. Shimizu, M. Takeuchi, K. Nakamura, and A. Yamada, "Some studies on SAW resonators and multiple-mode filters", in *Proc. 1976 IEEE Ultrason. Symp.*, pp. 297-302.

[38] H. A. Haus, "Modes in SAW grating resonators", *J. Appl. Phys.* **48**, 4955-4961 (1977).

[39] C. S. Hartmann, P. V. Wright, R. J. Kansy, and E. M. Garber, "An analysis of SAW interdigital transducers with internal reflections and the application to the design of single-phase unidirectional transducers", in *Proc. 1982 IEEE Ultrason. Symp.*, pp. 40-45.

[40] C. S. Hartmann and B. A. Abbott, "A generalized impulse response model for SAW transducers including effects of electrode reflections", in *Proc. 1988 IEEE Ultrason. Symp.*, pp. 29-34.

[41] Y. Koyamada and S. Yoshikawa, "Coupled mode analysis of a long IDT", *Review of the Electrical Communication Laboratories* **27**, 432-444 (1979).

[42] D. P. Chen and H. A. Haus, "Analysis of metal-strip SAW gratings and transducers", *IEEE Trans. Sonics Ultrason.* **32**, 395-408 (1985).

[43] V. P. Plessky and C. S. Hartmann, "Characteristics of leaky SAWs on 36-$LiTaO_3$ in periodic structures of heavy electrodes" in *Proc. 1993 IEEE Ultrason. Symp.*, pp. 1239-1242.

[44] C. S. Hartmann and V. P. Plessky, "Experimental measurements of propagation, attenuation, reflection and scattering of leaky waves in Al electrode gratings on 41°, 52°, and 64°-$LiNbO_3$", in *Proc. 1993 IEEE Ultrason. Symp.*, pp. 1247-1250.

[45] K. Hashimoto, G. Q. Zheng, and M. Yamaguchi, "Fast analysis of SAW propagation under multi-electrode-type gratings with finite thickness", in *Proc. 1997 IEEE Ultrason. Symp.*, pp. 279-284.

[46] S. V. Biryukov and M. Weihnacht, "The effective permittivity in the complex plane and a simple estimation method for leaky wave slowness", in *Proc. 1996 IEEE Ultrason. Symp.*, pp. 221-224.

[47] P. Ventura, J. M. Hodé, and M. Solal, "A new efficient combined FEM and periodic Green's function formalism for the analysis of periodic SAW structures", in *Proc. 1995 IEEE Ultrason. Symp.*, pp. 263-268.

[48] P. Ventura, J. M. Hodé, M. Solal, and L. Chommeloux, "Accurate analysis of pseudo-SAW devices", in *Proc. 9th European Frequency and Time Forum* (1995), pp. 200-204.

[49] S. V. Biryukov, private communication.

[50] A. E. H. Love, *A Treatise on the Mathematical Theory of Elasticity* (Dover, 1944).

[51] L. D. Landau and E. M. Lifshitz, *Theory of Elasticity* (Pergamon Press, 1986).

[52] T. Ikeda, *Fundamentals of Piezoelectricity* (Oxford University Press, 1996).

[53] M. Buchner, W. Ruile, A. Dietz, and R. Dill, "FEM analysis of the reflection coefficient of SAWs in an infinite periodic array", in *Proc. 1991 IEEE Ultrason. Symp.*, pp. 371-375.

[54] U. Rösler, D. Cohrs, A. Dietz, G. Fischerauer, W. Ruile, P. Russer, and R. Weigel, "Determination of leaky SAW propagation, reflection and coupling on $LiTaO_3$", in *Proc. 1995 IEEE Ultrason. Symp.*, pp. 247-250.

[55] T. Sato and H. Abe, "Propagation of longitudinal leaky surface waves under periodic metal grating structure on lithium tetraborate", *IEEE Trans. Ultrason., Ferroelect., Freq. Contr.* **45**, 394-408 (1998).

[56] R. F. Milsom, N. H. C. Reilly, and M. Redwood, "Analysis of generation and detection of surface and bulk acoustic waves by interdigital transducers", *IEEE Trans. Sonics Ultrason.* **24**, 147-166 (1977).

[57] C. Wang and D. Chen, "Analysis of surface excitation of elastic wave field in a half space of piezoelectric crystal - general formulae of surface excitation of elastic field", *Chinese J. of Acoustics* **4**, 232-243 (1985).

[58] A. R. Baghai-Wadji, H. Reichinger, H. Zidek, and Ch. Mecklenbräuker, "Green's function applications in SAW devices", in *Proc. 1991 IEEE Ultrason. Symp.*, pp. 11-20.

[59] P. Ventura, J. Desbois, and L. Boyer, "A mixed FEM/analytical model of the electrode mechanical perturbation for SAW and PSAW propagation", in *Proc. 1993 IEEE Ultrason. Symp.*, pp. 205-208.

[60] P. Ventura, J.-M. Hodé, "A new accurate analysis of periodic IDTs. built on unconventional orientation on quartz", in *Proc. 1997 IEEE Ultrason. Symp.*, pp. 139-142.

[61] K. Hashimoto and M. Yamaguchi, "Precise simulation of surface transverse wave devices by discrete Green function theory", in *Proc. 1994 IEEE Ultrason. Symp.*, pp. 253-258.

[62] K. Hashimoto, G. Endoh and M. Yamaguchi, "Coupling-of-modes modelling for fast and precise simulation of leaky surface acoustic wave devices" in *Proc. 1995 IEEE Ultrason. Symp.*, pp. 251-256.

[63] K. Hashimoto and M. Yamaguchi, "General-purpose simulator for leaky surface acoustic wave devices based on coupling-of-modes theory", in *Proc. 1996 IEEE Ultrason. Symp.*, pp. 117-122.

[64] R. C. Peach, "A general Green function analysis for SAW devices", in *Proc. 1995 IEEE Ultrason. Symp.*, pp. 221-225.

[65] V. P. Plessky and T. Thorvaldsson, "Periodic Green's function analysis of SAW and leaky SAW propagation in a periodic system of electrodes on a piezoelectric crystal", *IEEE Trans. Ultrason., Ferroelect., Freq. Contr.* **42**, 280-293 (1995).

[66] A. Isobe, M. Hikita, K. Asai, "Propagation characteristics of longitudinal leaky SAW in Al-grating structure", *IEEE Trans. Ultrason., Ferroelect., Freq. Contr.* **46**, 849-855 (1999).

[67] B. Jakoby and M. J. Vellekoop, "FFT-based analysis of periodic structures in microacoustic devices", *IEEE Trans. Ultrason., Ferroelect., Freq. Contr.* **47**, 651-656 (2000).

[68] O. Kawachi, G. Endoh, M. Ueda, O. Ikata, K. Hashimoto, and M. Yamaguchi, "Optimum cut of $LiTaO_3$ for high performance leaky surface acoustic wave filters", in *Proc. 1996 IEEE Ultrason. Symp.*, pp. 71-76.

[69] K. Hashimoto, M. Yamaguchi, S. Mineyoshi, O. Kawachi, M. Ueda, G. Endoh, and O. Ikata, "Optimum leaky-SAW cut of $LiTaO_3$ for minimised insertion loss devices", in *Proc. 1997 IEEE Ultrason. Symp.*, pp. 245-254.

[70] M. P. da Cunha and S. de A. Fagundes, "Investigation on recent quartz like materials for SAW applications", in *Proc. 1998 IEEE Ultrason. Symp.*, pp. 283-288.

[71] I. M. Silvestrova, V. V. Bezdelkin, P. A. Senyushenkov and Yu. V. Pisarevsky, "Present stage of $La_3Ga_5SiO_{14}$ -research", in *Proc. 1993 International Freq. Contr. Symp.*, pp. 348-350.

[72] S. Sakharov, P. Senyushenkov, A. Medvedev and Yu. Pisarevsky, "New data on temperature stability and acoustical losses of langasite crystals", in *Proc. 1995 International Freq. Contr. Symp.*, pp. 647-652.

[73] V. P. Plessky, D. P. Chen, and C. S. Hartmann, "'Patch' improvements to COM model for leaky waves", in *Proc. 1994 IEEE Ultrasonics Symposium*, pp. 297-300.

[74] K. Hashimoto, J. Koskela, and M. M. Salomaa, "Fast determination of coupling-of-modes parameters based on the strip admittance approach", in *Proc. 1999 IEEE Ultrason. Symp.*, pp. 93-96.

[75] Z. H. Chen and K. Yamanouchi, "Theoretical analysis of relations between directivity of SAW transducer and its dispersion curves", in *Proc. 1989 IEEE Ultrason. Symp.*, pp. 71-74.

[76] S. Datta, and B. Hunsinger, "First-order reflection coefficient of surface-acoustic waves from thin-strip overlays", *J. Appl. Phys.* **50**, 5661-5665 (1979).

[77] B. A. Auld, and D. F. Thompson, "Temperature compensation of surface transverse waves for stable oscillator applications", in *Proc. 1987 IEEE Ultrason. Symp.*, pp. 305-312.

[78] E. Gavignet, S. Ballandras, and E. Bigler, "Theoretical analysis of surface transverse waves propagating on a piezoelectric substrate under shallow groove or thin metal strip gratings", *J. Appl. Phys.* **77**, 6228-6233 (1995).

[79] E. J. Danicki, "Propagation of transverse surface acoustic waves in rotated Y-cut quartz substrates under heavy periodic metal electrodes", *IEEE Trans. Sonics Ultrason.* **30**, 304-312 (1983).

[80] V. P. Plessky, "Two parameter coupling-of-modes model for shear horizontal type SAW propagation in periodic gratings", in *Proc. 1993 IEEE Ultrason. Symp.*, pp. 195-200.

[81] J. L. Bleustein, "A new surface wave in piezoelectric crystals", *Appl. Phys. Lett.* **13**, 412-413 (1968).

[82] K. Yamanouchi and K. Shibayama, "Propagation and amplification of Rayleigh waves and piezoelectric leaky surface waves in $LiNbO_3$", *J. Appl. Phys.* **32**, 856-862 (1972).

[83] K. Nakamura, M. Kazumi, H. Shimizu, "Surface and Rayleigh-type surface waves on rotated Y-cut $LiTaO_3$", in *Proc. 1977 IEEE Ultrason. Symp.*, pp. 819-822.

[84] A. E. H. Love, *Some Problems of Geodynamics* (Cambridge University Press, 1911; Dover, 1967).

[85] B. A. Auld, J. J. Gagnepain, and M. Tan, "Horizontal shear waves on corrugated surfaces", *Electron. Lett.* **12**, 650-651 (1976).

[86] Yu. V. Gulyaev and V. P. Plessky, "Slow acoustic surface waves in solids", *Sov. Tech. Phys. Lett.* **3**, 87-88 (1977).

[87] S. V. Biryukov, Yu. V. Gulyaev, V. V. Krylov, and V. P. Plessky, *Surface Acoustic Waves in Inhomogeneous Media* (Springer-Verlag, 1995). pp. 163-174.

[88] B. P. Abbott and K. Hashimoto, "A coupling-of-modes formalism for surface transverse wave devices", in *Proc. 1995 IEEE Ultrason. Symp.*, pp. 239-245.

[89] K. Hashimoto, *Surface Acoustic Wave Devices in Modern Communication Systems and their Simulation Technologies* (Springer-Verlag, 2000).

[90] Y. Sakamoto, K. Hashimoto, M. Yamaguchi, "Behaviour of leaky surface acoustic wave propagation at discontinuous region of periodic grating", *Jpn. J. Appl. Phys* **37**, 2905-2908 (1998).

[91] S. Krasnikova, B. P. Abbott, and R. C. Almar, "COM parameter extraction for STW resonator design", in *Proc. 11th European Frequency and Time Forum* (1997), pp. 440-444.

[92] V. L. Strashilov, K. D. Djordjev, and V. M. Yantchev, "The coupling-of-modes approach to the analysis of STW devices: part II", *IEEE Trans. Ultrason., Ferroelect., Freq. Contr.* **46**, 1512-1517 (1999).

[93] A. Rønnekleiv, "Anisotropy in surface transverse wave resonators", in *Proc. 1987 IEEE Ultrason. Symp.*, pp. 325-329.

[94] The test structure was designed, fabricated and measured by Thomson Microsonics, Sophia-Antipolis, France.

[95] H. H. Ou, N. Inose, and N. Sakamoto, "Improvement of ladder-type SAW filter characteristics by reduction of inter-stage mismatching loss", in *Proc. 1998 IEEE Ultrason. Symp.*, pp. 97-102.

[96] J. Knuuttila, P. Tikka, V. P. Plessky, T. Thorvaldsson, and M. M. Salomaa, "Recent advances in laser-interferometric investigations of SAW devices", in *Proc. 1997 IEEE Ultrason. Symp.*, pp. 161-164.

[97] J. V. Knuuttila, P. T. Tikka, C. S. Hartmann, V. P. Plessky, and M. M. Salomaa, "Anomalous asymmetric acoustic radiation in low-loss SAW filters", *Electron. Lett.* **35**, 1115-1116 (1999).

[98] C. S. Hartmann, V. P. Plessky, and S. Jen, "112°-$LiTaO_3$ periodic waveguides", in *Proc. 1995 IEEE Ultrason. Symp.*, pp. 63-66.

[99] S. Rooth and A. Rønnekleiv, "SAW propagation and reflections in transducers behaving as waveguides in the sense of supporting bound and leaky mode", in *Proc. 1996 IEEE Ultrason. Symp.*, pp. 201-206.

[100] M. Solal, J. Knuuttila, and M. M. Salomaa, "Modelling and visualization of diffraction like coupling in SAW transversely coupled resonators filters", in *Proc. 1999 IEEE Ultrason. Symp.*, pp. 101-106.

[101] P. Ventura, J. M. Hodé, and B. Lopes, "Rigorous analysis of finite SAW devices with arbitrary electrode geometries", in *Proc. 1995 IEEE Ultrason. Symp.*, pp. 257-262.

[102] R. Peach, "Green function analysis for SAW devices with arbitrary electrode structures", in *Proc. 1997 IEEE Ultrason. Symp.*, pp. 99-103.

[103] J. Desbois, private communication.

Abstracts of Publications I-VI

I We discuss effects on the propagation of surface acoustic waves (SAW) due to heavy mass loading on Y-cut lithium niobate and lithium tantalate substrates. An abrupt reduction in the leaky-SAW (LSAW) attenuation is observed in the measured admittance of a long resonator test structure on 64°-YX-cut lithium niobate for aluminum electrodes of thickness h/λ_0 beyond 9-10%. This experimental fact is explained theoretically as the slowing down of the leaky wave below the velocity of the slow shear surface-skimming bulk wave (SSBW), such that energy dissipation into bulk-wave emission becomes inhibited. An infinite transducer structure in modeled using the Green's function and the boundary-element method (BEM); the computed theoretical properties well explain for the experimental findings. The model is further employed to quantify the leaky surface-acoustic wave attenuation characteristics as functions of the crystal-cut angle and the thickness of the electrodes. The resonance and antiresonance frequencies and the corresponding Q values are investigated to facilitate the selection of the crystal cuts and electrode thicknesses. The transformation of the leaky SAW into a SAW-type non-leaky wave is also predicted to occur for gold electrodes, with considerably thinner finger structures.

II Surface transverse waves (STW) are numerically simulated on langasite. As our method of investigation, we compute the admittance of an infinite synchronous resonator. The resonance and antiresonance frequencies are evaluated as functions of the crystal cut, temperature and the thickness of the aluminium electrodes. For optimal parameters, we demonstrate a vanishing first-order temperature coefficient at room temperature and find a coupling strength several times stronger than that for Rayleigh waves in ST quartz. In particular, we find that the sensitivity of the resonance frequency to variations in the thickness of the aluminium electrodes is significantly lower in langasite than in ST quartz.

III A novel numerical method for determining the surface acoustic wave and the leaky surface acoustic wave characteristics is proposed. The Green's function method is used to simulate an infinite periodic transducer driven by a periodic voltage. We show that the coupling of modes parameters and the dispersion relation can be extracted from the change in the admittance as the periodicity of the driving voltage is slightly shifted. The method first introduced here leads to significant savings in computing time.

IV An analytic approach is developed for simulating synchronous resonators employing shear horizontally polarized surface acoustic waves, such as surface transverse waves, and leaky surface acoustic waves on $LiTaO_3$ and $LiNbO_3$ substrates. The approach, based on a simplified parametrized Green's function theory, allows the description of the localization of the wave and the interaction with bulk acoustic waves. An analytic expression is found for the harmonic admittance of an infinite periodic electrode array, and approximate corrections for finite structures are presented. The model enables fast computation of the admittance of synchronous resonators and it compares favorably with experiments and numerical simulations.

V We discuss an acoustic loss mechanism in surface-acoustic wave resonators on 36°YX-cut lithium tantalate substrate. Recent acoustic field scans performed with an optical Michelson interferometer reveal a spatially asymmetric acoustic field atop the busbars of a resonator, giving a rise to acoustic beams which escape the resonator area and lead to undesired losses. Here, we link the phenomenon with the inherent crystalline anisotropy of the substrate: the shape of the slowness curves and the asymmetry of the polarization for leaky surface-acoustic waves, propagating at an angle with respect to the crystal X-axis.

VI We discuss acoustic losses in synchronous leaky surface-acoustic wave resonators on rotated Y-cut lithium tantalate substrates. Laser probe measurements and theoretical methods are employed to identify and characterize the radiation of leaky waves into the busbars of the resonator and the excitation of bulk-acoustic waves. Escaping LSAWs lead to a significant increase in the conductance, typically occurring in the vicinity of the resonance and in the stopband, but they do not explain the experimentally observed deterioration of the electric response at the antiresonance. At frequencies above the stopband the generation of fast shear bulk-acoustic waves is the dominant loss mechanism.

Errata for Publications I-VI

The following misprints have been found in papers I-VI:

- **Paper I**
  - p. 441, Eq. (7) should read

$$\left[\begin{array}{c} \mathbf{T}(x) \\ \sigma(x) \end{array} \right]_{\omega} = \sum_{n=-\infty}^{+\infty} \left[\begin{array}{c} \mathbf{t}(x - n\lambda_0) \\ c(x - n\lambda_0) \end{array} \right]_{\omega}.$$

- **Paper II**
  - p. 2666, Eq. (2) should read

$$\frac{\delta f}{f_0} \equiv 2\,\frac{f_{ar} - f_r}{f_{ar} + f_r}.$$

- **Paper III**
  - p. 808, lines 4-6, the sentence beginning "Dividing the local current density ..." should be replaced [103] with "Integrating the local current density over a unit periodic we obtain:"
  - p. 808, Eq. (10) should read

$$Y(f,\beta) = \left[-i4\alpha^2\lambda_0 \frac{\delta - \kappa}{\delta^2 - \kappa^2 - \beta^2} + i2\pi f C_p \right] \frac{\sin(\beta p)}{\beta p}.$$

  - p. 808, after Eq. (10) it should read: "Since β is assumed small, the factor outside the brackets in the r.h.s. of (10) is almost unity and will from here on be ignored."

- **Paper V** - p. 2684, Fig. 2, the vertical axes should read (a) "$|\omega \mathrm{U}/\sigma|$ [Å^2/Cs]" and (b) "phase $\omega \mathrm{U}/\sigma$ [degrees]", and the caption should read "Computed polarization for LSAWs propagating on a metallized crystal surface at an angle θ with respect to the crystal X-axis: (a) the relative magnitude and (b) the relative phase of components of mechanical displacement, normalized to the angular frequency $\omega = 2\pi f$ and the charge density σ."